CONF-9505389--1

EVALUATION OF OXIDE DISPERSION STRENGTHENED (ODS) MOLYBDENUM ALLOYS

Robert Bianco and R. William Buckman, Jr.

DE-AC11-88PN38014

RECEIVED
JAN 15 1998
OSTI

MASTER

DISTRIBUTION OF THIS DOCUMENT IS UNLIMITED HH

BETTIS ATOMIC POWER LABORATORY WEST MIFFLIN, PENNSYLVANIA 15122-0079

Operated for the U.S. Department of Energy
by WESTINGHOUSE ELECTRIC CORPORATION

NOTICE

This report was prepared as an account of work sponsored by the United States Government. Neither the United States, nor the United States Department of Energy, nor any of their employees, nor any of their contractors, subcontractors, or their employees, makes any warranty, express or implied, or assumes any legal liability or responsibility for the accuracy, completeness or usefulness of any information, apparatus, product or process disclosed, or represents that its use would not infringe privately owned rights.

DISCLAIMER

This report was prepared as an account of work sponsored by an agency of the United States Government. Neither the United States Government nor any agency thereof, nor any of their employees, make any warranty, express or implied, or assumes any legal liability or responsibility for the accuracy, completeness, or usefulness of any information, apparatus, product, or process disclosed, or represents that its use would not infringe privately owned rights. Reference herein to any specific commercial product, process, or service by trade name, trademark, manufacturer, or otherwise does not necessarily constitute or imply its endorsement, recommendation, or favoring by the United States Government or any agency thereof. The views and opinions of authors expressed herein do not necessarily state or reflect those of the United States Government or any agency thereof.

DISCLAIMER

Portions of this document may be illegible electronic image products. Images are produced from the best available original document.

Abstract:

A series of fourteen (14) novel high-strength molybdenum alloy compositions containing a dispersion of very fine (< 1 μm diameter) oxide particles were consolidated using two proprietary powder metallurgy techniques. The developmental compositions were evaluated to determine the microstructural stability and mechanical properties from cryogenic (-148°F) to elevated temperatures (4000°F) for material in the as-swaged (>98% cold work) condition and for as-swaged material in the heat treated condition. Extremely fine oxide particle sizes (<1000 Å) were observed by Transmission Electron Microscopy (TEM) for a number of the experimental compositions in the as-swaged condition. A one hour recrystallization temperature as high as 3990°F was measured and a ductile-to-brittle transition temperature as low as -58°F for material in the recrystallized condition was determined. The preliminary results support the alloy design concept feasibility.

Introduction:

Commercially available molybdenum-base alloys do not possess sufficient creep or tensile strength to survive operating temperatures at or above 2400°F (0.5 T_m) for long-term service applications. The commercially available Mo-TZM and Mo-TZC alloys, strengthened by a combination of solid-solution strengthening additions and carbide particles (precipitation strengthening) plus thermomechanical processing, lose their desired mechanical properties in relatively short time periods above these temperatures. The development of a thermally stable and high-strength, molybdenum-base alloy, such as the oxide dispersion strengthened (ODS) molybdenum alloy presented herein, will extend the lifetime or replace other material systems for a number of applications. The following is a partial list:

COMMERCIAL:

- Heating Elements
- Radiant Heat Shields
- Electrical Posts for Lamp Filaments

SPACE NUCLEAR POWER AND PROPULSION SYSTEMS:

- High Temperature Springs
- High-Strength Fiber Reinforcements for:
  - High Temperature Heat Exchanger
  - Blades and Vanes for Brayton and Rankine Cycle Turbines
  - Regeneratively Cooled Rocket Nozzles
  - Rocket Combustion Chambers
  - Blades and Vanes for Advanced Space Shuttle Main Engines

AEROSPACE:

- High-Strength Fiber Reinforcements for:
  - Regeneratively Cooled Rocket Nozzles
  - Rocket Combustion Chambers

- Blades and Vanes for Hypersonic Engine Compressors/Turbines
- Blades, Vanes, and Structurals for High Speed Civilian Transport Engine
- Airframe Structural Members

- High-Strength Dies for Isothermal Forging of Nickel- and Cobalt-Base Superalloy Components for Aircraft Gas Turbine Engines

COMMERCIAL NUCLEAR FUEL:

- Creep Resistant Boats for Fuel Sintering

Molybdenum, a refractory metal from Group VI of the Periodic Table, can be strengthened by (a) solid-solution strengthening additions, (b) precipitation or dispersion strengthening by second-phase particles, (c) strain hardening and grain size refinement, and (d) retaining a worked structure at high temperatures. For service at elevated temperatures ($>0.5T_m$), only a combination of (b), (c), and (d) has the potential for success.

Strengthening by second-phase particles can be both direct and indirect as demonstrated for the SAP (sintered aluminum product) and TD (thoria dispersion strengthened) Nickel and TD Nichrome alloys. Direct strengthening is caused by particles acting as barriers to dislocation motion during deformation. Indirect strengthening is caused when a dispersoid-containing metal is thermomechanically processed, so that the particles help to develop and stabilize a worked structure. An additional strength increment resulting from the fine grain size and substructure can be achieved at high temperature if the structure is stable. Carbides have been the favored second-phase particle for strengthening molybdenum, as is evident in the Mo-TZM and Mo-TZC type alloys. However, the carbide particles are not stable at high temperature and will coarsen and/or dissolve into solution, thereby negating their effectiveness as a strengthener. Inert oxide particles are preferable as the dispersoid. In earlier work where the oxide particles were added by mechanical blending, the particle sizes were generally too coarse, particle diameter $> 1\mu$, and thus optimum strengthening could not be achieved, Reference (a). In fact, very fine dispersions of thoria, particle diameter $\approx$ 400Å, in tungsten were achieved and the high temperature strength (tensile and creep) of pure tungsten was increased significantly, Reference (b). The fine thoria dispersion was achieved by chemical introduction of thoria via a nitrate salt which formed thoria by pyrolysis during the hydrogen reduction of the ammonium paratungstate at 1650°F.

Problem:

Traditionally, cold-worked metals heated to $0.5T_m$ and above tend to recrystallize (i.e. reform an equiaxed microstructure) and lose any benefit of the prior thermomechanical processing. The effectiveness of a thoria particle dispersion in a tungsten matrix was demonstrated to temperatures of 5070°F which is $0.84T_m$ of tungsten. Thus, if similar improvements can be achieved in molybdenum, the cold-worked structure could be stable at temperatures up to approximately 3900°F.

Tungsten, molybdenum, or their alloys--which are processed using powder-metallurgy techniques--are excellent candidates for oxide dispersion strengthening (ODS) because these metals have very low solubility for oxygen and only moderate affinity to form oxides. The first oxide dispersion strengthened tungsten alloys containing a coarse, thermodynamically stable oxide (e.g. thoria, ThO_2) particle addition were developed to improve electron emission properties for use as welding rod in the gas tungsten arc (GTA) and other welding processes. However, ODS tungsten alloys containing a finer thoria particle were produced with excep-

tional creep strength and microstructural stability (i.e. recrystallization temperature, grain growth, etc.) up to 80% of the melting temperature, Reference (b). In fact, the creep strength (i.e. stress to give 1% creep strain in 1,000 hours) of thoriated tungsten alloys was measured to be up to five times higher than commercially-pure tungsten. These alloys are used in several high-temperature applications such as lamp filaments which have improved resistance to shock loading during service, rocket nozzle inserts, and missile nose tips.

Commercially pure molybdenum, on the other hand, has a recrystallization temperature between 1600°F ($0.3T_m$) and 2300°F ($0.5T_m$). Cold-worked pure molybdenum will exhibit poor long-term creep properties above 2000°F because the cold-worked microstructure is not stable and will recrystallize during service, Reference (c). Schwarzkopf Development Corporation, a commercial molybdenum alloy supplier, has patented a mechanical preparation method or dry blended process, whereby a powder mixture of molybdenum and a desired oxide (~2 μm diameter) or a low temperature decomposable hydroxide or carbonate oxide compound are mixed, Reference (d). The resulting powder batch mixture is then cold isostatically pressed (CIP), hydrogen sintered, and processed to wire or sheet. The steady-state creep rates of this ODS molybdenum alloy ($1.3x10^{-5}$ and $7.6x10^{-5}$ hr^{-1}) measured from constant load (~4.3 ksi) uniaxial creep tests conducted at 2820°F and 3180°F in vacuum were at least 3.5 orders of magnitude lower than commercially pure molybdenum ($5.5x10^{-2}$ and $7.1x10^{-1}$ hr^{-1}). A graphic comparison of the creep rates of these materials with data from molybdenum-niobium alloy single crystals are presented in Figure 1. The creep rate of the dry blended, ODS molybdenum alloy was considerably lower at 2820°F and nearly equivalent at 3180°F compared to a single crystal molybdenum-niobium alloy, Reference (e).

A technique has been developed for producing a fine-grained molybdenum alloy containing a dispersion of fine (~0.1 μm diameter), inert oxide particles. A fine-grained microstructure improves both ductility and fracture toughness, whereas a dispersion of fine oxide particles (i.e. a large particle density and small interparticle spacing) impedes both grain boundary and dislocation mobility. For service conditions above $0.5T_m$, creep deformation is dependent on these mobilities and would, therefore, be strongly improved by the presence of a finer oxide particle dispersant, Reference (f). A series of experimental ODS molybdenum alloys containing fine particle additions of lanthana, yttria, ceria, and thoria were consolidated, processed to rod, and evaluated, as outlined in Table 1. The results of optical and electron (TEM) microscopy analyses, vacuum annealing studies, and uniaxial tensile tests of as-swaged and vacuum annealed alloys are presented herein.

Experimental Procedure:

MATERIAL PREPARATION:

Alloy Preparation: For this program, development of a series of experimental ODS molybdenum alloys having lanthana, yttria, ceria, and thoria additions was undertaken (Table 1). Except for thoria containing alloys, these alloys were fabricated by Philips-Elmet, Corp. in Lewiston, ME, a well-established tungsten alloy vendor. Two concentration levels of oxide dispersants in each molybdenum alloy were prepared using one of two proprietary powder metallurgy techniques. Alloy powder mixtures were ball milled, cold isostatically pressed (CIP) at 35,000 psi for at least fifteen minutes into billets weighing approximately 8 pounds and measuring 1.5 inches in diameter, and then sintered between 3450° and 3540°F for 3-7 hours in a hydrogen atmosphere. Finally, the as-sintered billets were preheated under a hydrogen atmosphere, hand and machine swaged to 0.285 inch diameter, and then cold drawn to a 0.156-0.163 inch final diameter. The complete details of the swaging and drawing operations are listed in Table 1. The total percent of strain-hardening following the swag-

ing/drawing steps was about 98.1%. An in-process anneal at 3270°F for one minute was performed on the first ingots of the yttria alloys following machine swaging to a 0.300 inch diameter. The resulting rods were then straightened, sectioned into seventy-three inch lengths, cleaned in a caustic bath of fused potassium hydroxide to remove 0.001-0.003 inches from the diameter, trimmed, and finally eddy current (NDE) tested prior to shipment.

Test Specimen Preparation: Room and elevated temperature tensile specimens were machined to a four microinch surface finish according to Figures 2a and 2b, respectively. One specimen, machined from each one of the ODS molybdenum alloy compositions, was electropolished in a room temperature solution containing 4 parts concentrated sulfuric acid and 1 part distilled water using a Type 304 stainless steel cathode and a direct current accelerating potential of 6-7 volts to remove 1-2 mils from the diameter.

MATERIAL CHARACTERIZATION:

Physical Properties: The average density of each as-sintered alloy billet, intermediate swaged rod, and fully swaged/drawn alloy rod was measured using the Archimedes principle (wet-dry method). The wet-dry method or the Archimedes principle is used to determine the volume of an irregularly shaped sample by measuring the amount of water displaced from a wet (submerged) sample while knowing the density of the fluid. In this case, water was used with three drops of a surfactant to facilitate wetting of the sample surface. An average from at least four samples of the intermediate and fully swaged/drawn alloy rod was measured. The average density of the as-sintered alloy ingots was measured and provided by the vendor (Philips-Elmet).

Chemical Analysis: Chemical analysis of each ODS molybdenum alloy composition was performed at Teledyne Wah Chang Albany, Albany, OR. Direct current plasma (DCP) spectrometry was used to measure the amount of the oxide dispersant and major impurity levels (i.e. iron, nickel, chromium, copper, and potassium).

Based on initial optical metallography, transmission electron microscopy (TEM) analysis was also completed on selected alloy compositions at the Alcoa Technical Center, Alcoa Center, PA.

TEM Thin Foil Preparation: Longitudinal and transverse thin foil specimens from selected ODS alloy compositions were prepared by sectioning with a low-speed diamond saw, mechanically thinning by grinding on silicon carbide paper, and polishing with fine diamond paste. A room temperature solution containing 1 part concentrated sulfuric acid and 7 parts methanol operated at a direct current accelerating potential of 15 V and a current density of 150 mA/cm^2 was used to thin each specimen until perforation. Ion milling using argon ions at an accelerating potential of 4 kV and with either 15° or else 11° incident angle was used to complete the final stages of thinning and polishing, respectively. The thinned areas around the perforation were approximately 500 - 1500 Å thick.

TEM Examination: Thin foils were characterized using a Philips EM420 transmission electron microscope (TEM) with an accelerating potential of 120 kV. Brightfield (BF) and darkfield (DF) micrographs were taken to document the shape and size of the strain-hardened microstructure and oxide particles, respectively. Selected area electron diffraction (SAED) techniques were also used to identify the oxide phase/crystallography and the preferred grain oreintation of the as-swaged ODS molybdenum alloys.

MICROSTRUCTURAL STABILITY PROPERTIES:

The following tests were performed on the ODS molybdenum alloys to determine the thermal stability (recrystallization temperature) of the strain-hardened microstructure and to measure the physical (density) and mechanical properties (tensile strength). The recovery properties (i.e. Knoop microhardness versus annealing temperature) and recrystallization temperatures of as-swaged rod were measured by heating each alloy for one hour under dynamic vacuum ($<10^{-5}$ torr) between 2010° and 3992°F in 180°F intervals. As-swaged and annealed specimens of each alloy were prepared for optical microscopy by sectioning, mounting in Bakelite, and polishing through a series of declining grit sizes. The final relief polish used 0.05 micron alumina powder. The mounts were swab etched with Murakami's etchant (10 gms potassium ferricyanide, 10 gms potassium hydroxide, and 100 ml distilled water). The average of at least five Knoop microhardness (KHN) indents along the longitudinal section of each metallographically prepared specimen was measured using an automated micro-hardness tester, Wilson Tukon 200. A diamond indenter with a 500 gram load and a ten second dwell time was used. In addition, the average bulk hardness of at least five Vickers microhardness indents along the transverse and longitudinal orientations was also measured using a manual microhardness machine. A diamond pyramid indenter with a five kilogram load and a ten second dwell time was used. The average grain size of as-sintered ingots and the average grain width of as-swaged rods were measured using the linear intercept method, according to ASTM standard E89. The average size and shape of the oxide particles was determined from unetched optical micrographs using a similar method.

MECHANICAL PROPERTIES:

Ductile-to-Brittle Transition Temperature (DBTT): The following mechanical properties were measured from the ODS molybdenum alloy rods: (a) 0.2% offset yield stress, (b) ultimate tensile stress, (c) percent reduction in area (measured from electron micrographs, SEM images), and (d) uniform and total elongation to failure. Round bar, tensile specimens of each as-swaged and selected alloy compositions vacuum annealed at 3630° ±5°F for one hour were loaded uniaxially to failure following a thirty minute soak per ASTM specification E21 and a temperature range between 212° and -148°F and a strain rate of 0.05 min^{-1} or $8.33x10^{-4}$ sec^{-1} to determine the ductile-to-brittle transition temperature. The fracture surface was analyzed with a scanning electron microscope (SEM), Amray model 1810, to identify the type of fracture; i.e. ductile or dimpled, cleavage, intergranular, or mixed-mode; and to determine the DBTT.

Elevated Temperature Tensile Tests: Elevated temperature tensile specimens of each as-swaged alloy were equilibrated at 2910°, 3270°, 3630°, and 3990°F±5°F for thirty minutes in vacuum ($<10^{-5}$ torr) and then loaded uniaxially to failure at a strain rate of 0.05 min^{-1} or $8.33x10^{-4}$ sec^{-1}. The fracture surface was again analyzed with the SEM to identify the type of fracture. In addition, fractured specimens were prepared metallographically and examined optically. Elevated temperature tensile tests are an effective and economical technique for properly screening candidate alloys, since creep strengths for the Group VI elements are related to these properties.

Experimental Results and Discussion:

MATERIAL CHARACTERIZATION:

Physical Properties: The average measured densities of the as-sintered alloys ranged between 93.4 and 98.9% of the theoretical density (TD) calculated for each alloy composition. Two exceptions were noted: the two and four volume percent yttria, wet-doped alloys were 83.6% and 81.8% TD after conventional sintering. These low density alloys were not

processable because of numerous cracks during swaging. Therefore, an alternate process was adopted. These alloys were swaged and resintered (twice) alternately until the diameter was one inch. At this time, the average measured densities of the wet-doped yttria alloys ranged between 98 and 99% TD, which was suitable for subsequent normal processing. The average measured densities of the remaining as-swaged alloys ranged between 99.1 and 100.6% TD. The theoretical density of these alloys is assumed to be a weighted average of the oxide dispersant and molybdenum theoretical densities according to the law of mixtures. Measured densities in excess of 100% may have resulted from either an error in the density measurement, the presence of a second-phase present in the alloy which was not accounted for in the calculation, or the presence of a substoichiometric oxide. No significant porosity was observed during optical metallographic examination, except for the pull-out of oxide particles from the molybdenum matrix. However, during the transmission electron microscopy (TEM) examination of as-swaged ODS alloy compositions, microvoids were detected between oxide dispersants and the molybdenum matrix.

The density of intermediate swaged ODS molybdenum alloy rods containing lanthana and ceria dispersants was also measured. The average densities of these alloys ranged between 99.7 and 100.7% TD. Therefore, densification occurred prior to the final swaging and cold drawing operations. Optical metallographic examination of these samples again failed to identify any porosity.

Chemical Analysis: The results of chemical analysis conducted at Teledyne Wah Chang Albany are presented in Table 3. With the exception of the 4LD and 4LW compositions, all lots were reasonably close to the targeted two and four volume percent dispersant levels. The lower than desired volume fractions obtained on the four volume percent alloys containing lanthana probably resulted from the slightly lower melting temperature (e.g. La_2O_3 = 4100°F; CeO_2 = 4530°F; Y_2O_3 = 4405°F) causing evaporation during sintering.

Microstructural Characterization: A representative optical micrograph of as-swaged alloys containing two volume percent ceria dispersants and processed using Procedure A and B are presented in Figures 3 and 4. The microstructure of the as-swaged ODS alloys are characterized by refined and elongated grains with an average grain width ranging between 1.0 and 30.0 μm. The average aspect ratio (average grain length/average grain width) were extremely difficult to measure optically because the length and width of these elongated grains were difficult to distinguish. The average aspect ratio was also impossible to measure in the TEM because the length of grains extended beyond the diameter of the TEM foil. However, the aspect ratio of vacuum annealed elongated grains were between 10/1 - 100/1. The average grain size of as-sintered, intermediate swaged, and fully swaged/drawn ODS molybdenum alloys are compared in Tables 4 and 5. The size and shape of the oxide dispersants are also listed in Table 4 and classified into two groups: non-deformable, spherical particles (e.g. yttria ODS alloys) and deformable stringers (e.g. lanthana and ceria ODS alloys). During swaging, the oxide particle size is sequentially reduced to the fully swaged condition, compare Figures 3 and 5. The shape of the oxide particles within the as-sintered alloys were blocky or generally spherical. However, following the swaging and drawing processes, the softer lanthana and ceria particles plastically deformed into stringers which even segmented into smaller more spherical particles (Figures 3 and 5). The size and shape of the harder yttria particles, on the other hand, remained unchanged. Overall, Procedure B produced ODS alloys, especially for the ceria and lanthana dispersants, with a much finer (between 0.05 and 0.5 μm diameter) particle size compared to the Procedure A alloys (1-10 μm diameter). An ODS alloy with a finer oxide particle size exhibits a greater particle density (N_v=no./volume) and a smaller average interparticle spacing (0.8-1.5 μm). Particle density, in particles/cm^3, is directly related to the ratio of volume fraction, f, and the average volume/particle, Eq. 1.

$$N_v = f/\{(4/3)\pi r^3\} \qquad [1]$$

where r is the average oxide particle radius, Reference (f). Genereally, the average particle density increased as the particle diameter decreased and the volume fraction increased. The ODS molybdenum alloys via Procedure B produced a finer oxide particle size and larger density compared to alloys via Procedure A. A finer, second-phase particle is expected to interact or impede the motion of mobile dislocations and grain boundaries better than a larger oxide particle size, causing an effective increase in the thermal stability of a strain-hardened microstructure (i.e. increased recrystallization temperature) and creep strength.

The purpose of the TEM examination was to measure the average grain aspect ratio (length/width) or width and the oxide particle size, shape, distribution, and interparticle spacing using both brightfield (BF) and darkfield (DF) images. Representative longitudinal and transverse transmission electron micrographs (TEM) of selected ODS molybdenum alloys via Procedure B are presented in Figures 6 and 7. Microvoids between the oxide particle and the molybdenum matrix were observed in the ODS alloys containing the non-deformable yttria particle, Figure 8. In addition, using selected area electron diffraction (SAED) analysis, the oxide structure and the preferred grain orientation of the above as-swaged alloy rods were identified. The results of this examination are summarized in Table 5. SAED results identified the cubic phases of Y_2O_3 and a microcrystalline phase of La_2O_3. However, SAED results identified the monoclinic phase of Ce_6O_{11}, instead of the cubic CeO_2 phase. XRD analysis confirmed that CeO_2 was the oxide phase in both the starting powder and the alloy powder batch mixture. The Ce_6O_{11} phase is a high temperature phase existing between 1450° and 1560°F, Reference (g). The CeO_2 phase readily transforms into the Ce_2O_3 phase in oxygen at temperatures above 2190°F or in reducing atmospheres without a temperature limit, Reference (h). In fact, cerium dioxide (CeO_2) particles dispersed in a tungsten welding rods, developed in Japan, were observed to transform into the Ce_2O_3 phase during sintering and swaging in hydrogen, Reference (i). ODS alloys containing cerium dioxide particle dispersants are sintered in hydrogen between 3450° and 3540°F and swaged between 2190° and 2510°F. Transformation of the CeO_2 phase to the Ce_2O_3 phase is possible; however, neither of these phases were identified in the as-swaged rod. The Ce_6O_{11} phase may just be a transition phase between complete transformation of CeO_2 to Ce_2O_3. A possible mechanism of this overall transformation is given below:

$$6CeO_2(s) + H_2(g) \rightarrow Ce_6O_{11}(s) + H_2O(g) \qquad [2a]$$

$$Ce_6O_{11}(s) + 2H_2(g) \rightarrow 3Ce_2O_3(s) + 2H_2O(g) \qquad [2b]$$

MICROSTRUCTURAL STABILITY PROPERTIES:

The only important strengthening mechanism in pure metals at ambient and elevated temperature is work- or strain-hardening and the subsequent retention of a strain-hardened (elongated) microstructure at elevated temperature. During strain-hardening, the yield and tensile strengths and electrical resistivity are increased due to the generation of dislocations and the refinement (elongation) of the microstructure, whereas the ductility and, in some cases, the resistance to corrosive attack are dramatically reduced. Following subsequent thermal exposures (annealing), the material slowly reverts back to its pre-hardened condition. These processes are referred to as recovery, recrystallization, and grain growth. Recovery is the process whereby a small amount of the stored energy of cold work is released resulting from the rearrangement of mobile dislocations into distinct cells and the annihilation of excess vacancies. During recovery, no significant change in microstructure or mechanical properties occurs; however, there is a marked decrease in the electrical resistivity of the

material. Recrystallization is the process which follows recovery whereby the remaining stored energy of cold work is released resulting in a dramatic change in the microstructure and mechanical properties of the cold-worked material. Recrystallization is characterized by the nucleation and growth of new, strain-free grains, a decrease in the yield and tensile strengths due to the annihilation of dislocations and grain growth, and an increase in the ductility and corrosion resistance of the material. The recrystallization temperature is defined as the temperature at which a material in a highly cold-worked state fully recrystallize (i.e. nucleates and grows a new, strain-free equiaxed grain) in one hour. Experimentally, the recrystallization temperature is determined by both a decrease or drop in the as-hardened microhardness and the presence of new, strain-free equiaxed grains. The last process is grain growth. Grain growth is the preferential increase in the average grain diameter of the material. The thermodynamic driving force for grain growth is the reduction in grain boundary area and the subsequent decrease in the surface energy of the boundary. Grain growth is also characterized by a softening or decrease in the yield and ultimate tensile strengths of the material.

The recrystallization temperature (RXT) and stability of the as-swaged microstructure was determined following one hour vacuum ($<10^{-5}$ torr) anneals at temperatures between 2010° and 3990°F at intervals of 180°F. Representative optical micrographs of the post-anneal samples are presented in Figures 9 and 10. The recrystallization temperatures measured from both microstructure and microhardness changes of each alloys are listed in Table 6. Five alloy compositions--2 and 4 vol.% ceria, Procedure B; 2 and 4 vol.% lanthana, Procedure B; and 4 vol.% lanthana, Procedure A--were identified which have RXT greater than both unalloyed and alloyed molybdenum (TZM and TZC) and a carbide-dispersion strengthened molybdenum-2.0 wt. rhenium alloy. The RXT of commercial unalloyed molybdenum is between 1600° and 2300°F depending on the purity of interstitials, strain and strain hardening rates, time at temperature during forming, and applied stress; whereas the RXT of commercial molybdenum alloys is between 2450° and 2800°F, Reference (c). In fact, three alloy compositions were identified with RXT nearly 85% of the melting temperature (Table 6). As for other ODS systems, RXT in excess of 80% of the melting temperature are typical. For instance, the RXT for TDNi (ODS thoria-nickel alloy) and ThDW (ODS thoria-tungsten alloy) are 2465°F (1350°C) and 5250°F (2900°C), respectively (Reference (b)).

The four most accepted nucleation models for producing strain-free grains are:

- polygonization,
- coalescence of neighboring subgrains,
- strain-induced boundary migration (SIBM), and
- martensitic (shear) transformation.

From all of these models, nucleation originates at a region where the local degree of deformation is highest, such as a grain boundary or dislocation, and requires the movement of this region into a region of less deformation until consumed. Therefore, the presence of a fine oxide particle and close interparticle spacing, giving a relatively high particle density, can effectively immobilize dislocations and grain boundaries, reducing substantially the nucleation rates in these alloys. On the other hand, the presence of a coarse oxide particle, large interparticle spacing, and consequently a smaller particle density can moderately impede grain boundary and dislocation mobility. However, a large oxide particle would also generate a locally high region of deformation during processing and, thus, can itself be an active site for the nucleation of a strain-free grain. Therefore, a coarse oxide dispersant will either be ineffective or else lower the RXT of these ODS molybdenum alloys. Nevertheless, once nucleation occurs, oxide particles of both sizes can inhibit grain boundary mobility (i.e. growth).

Anisotropic Recrystallization: In addition, two ODS molybdenum alloys compositions containing 2 and 4 volume percent of ceria or lanthana produced via Procedure B undergo anisotropic recrystallization. Anisotropic recrystallization is a term used to describe the movement of the recrystallization front/boundary in a preferred direction, producing a coarse elongated but softer (microhardness) microstructure (Figure 10). The recrystallization of an equiaxed microstructure is inhibited either from a physical barrier to lateral growth such as second phase and/or from the release of an excessive amount of stored energy promoting directional growth, Reference (j). In the case of the ODS alloys cited above, the oxide particles are not deformed during processing and are plastically deformed into elongated oxide stringers. These stringers inhibit lateral recrystallization growth and promote directional recrystallization. The affect of anisotropic recrystallization on mechanical properties remains to be evaluated.

MECHANICAL PROPERTIES:

Ductile-to-Brittle Transition Temperature (DBTT): The DBTT of each as-swaged and vacuum annealed alloy was determined by uniaxially loading a tensile specimen to failure at an ambient temperature range between 212° and -148°F and by measuring the 0.2% offset yield stress, ultimate tensile stress, the percent uniform elongation, the percent elongation to failure, and the reduction in area (measured from electron micrographs, i.e. SEM images). The room temperature tensile data of all the as-swaged ODS alloy compositions and selected alloy compositions vacuum annealed at 3630°F for one hour are presented in Tables 7 and 8, respectively. In addition, the effect of temperature and microstructure on the tensile properties of an ODS alloy containing two volume percent ceria via Procedure B in the as-swaged condition or vacuum annealed are compared in Figures 11 and 12. At room temperature, the elongations to failure of the as-swaged alloys ranged between 6 and 15%; whereas, the vacuum annealed alloys ranged between 8 and 39%, falling sharply as the DBTT is approached.

The DBTT of as-swaged and vacuum annealed ODS molybdenum alloys is listed in Table 9. The as-swaged ODS molybdenum alloys remained ductile and, probably, formable to temperatures well below room temperature (≤-58°F). However, two of the vacuum annealed ODS molybdenum alloys (i.e. 4 vol.% ceria and lanthana, Procedure B) remained ductile to temperatures below room temperature (Figure 13), whereas the remaining three alloys (i.e. 2 vol.% ceria and lanthana and 2 and 4 vol.% yttria, Procedure B) were not ductile at room temperature (Figure 14). Except for the ODS alloys containing 4 volume percent ceria and lanthana particles via Procedure B, the microstructures of the vacuum annealed alloys were fully recrystallized. This coarse grain size allows for a greater concentration of dislocation pileups at grain boundaries as well as lowering the number of dislocation sources available to accommodate slip, i.e. plastic deformation. For the as-swaged alloys, the alloys via Procedure B generally failed in a brittle manner (i.e. cleavage fracture, Figure 15) at -103°F (-75°C), whereas the alloys via Procedure A were still at least 80% ductile (i.e. dimpled fracture, Figure 16). In fact, coarse oxide particles were observed within the dimples (valleys) of the fracture surface. The strengths and microhardnesses of the as-swaged alloys via Procedure B were significantly higher compared to the alloys via Procedure A, indicating that this material strain hardened more rapidly (i.e. generated a larger dislocation density) and would probably exhaust its ductility and be more temperature dependent. Nevertheless, these alloys were substantially more ductile and formable than any tungsten-base system.

Elevated Temperature Tensile (ETT) Tests: The ETT properties of each as-swaged alloy were determined by uniaxially loading a stress rupture specimen to failure at 2910°, 3270°, 3650°, and 3990°F. A graphic comparison of the ultimate tensile strengths of the alloys produced

via Procedures A and B with an arc-cast, unalloyed molybdenum and commercially-pure powder metallurgy (CPPM) tungsten rod (1/2 inch diameter) in the as-rolled condition is presented in Figures 17 and 18, References (c) and (f). The arc-cast molybdenum and powder metallurgy tungsten specimens were held in a vacuum ($<10^{-4}$ torr) for fifteen minutes at temperature between 2500° and 3600°F and then loaded to failure at a crosshead speed of 0.0625 in/min. However, the UTS of unalloyed molybdenum is expected to decrease exponentially to zero at the melting temperature (4740°F). This trend was illustrated by dotted lines in Figures 17 and 18. For unalloyed molybdenum, the ultimate tensile stress (UTS) is directly related (about ten times greater) to the creep stress necessary to produce one percent plastic strain at the same temperature. However, as with other ODS systems, the UTS of ODS alloys reach a limit between 40 and 70 percent of the melting temperature, whereby the inert oxide particle continues to strengthen (Orowan mechanism) the matrix, Reference (b). Therefore, for these alloys, the relationship between the UTS and the creep stress necessary to produce one percent plastic strain may be greater than ten percent.

Note: The load applied during each tensile test was parallel to the direction of cold work and, where applicable, to the direction of recrystallization (i.e. anisotropic recrystallized grains). Therefore, as mentioned above, the isotropy of mechanical properties of these ODS alloy compositions remains to be evaluated.

The elevated temperature tensile specimens failed intergranularly. Representative electron micrographs (SEM) of the fracture surface and cross-sectional optical micrographs are presented in Figures 19 and 20. Decohesion of grains was observed throughout the region of plastic instability, i.e. the "necked" region. Generally, retaining a fine grain size/microstructure improved the elevated temperature tensile properties.

Summary:

The mechanical and physical behavior results indicate that Oxide Dispersion Strengthened (ODS) molybdenum alloys appear to be an excellent candidate for extended elevated temperature applications. Two powder metallurgy techniques were used to produce fifteen (15) ODS molybdenum alloy compositions. One technique, Procedure B, incorporated a fine (< 0.5 μm particle diameter) oxide particle dispersion. Alloy compositions were identified which retain a high-strength, strain-hardened microstructure up to 4000°F and are expected to have superior creep strength relative to unalloyed molybdenum. In addition, all as-swaged ODS molybdenum alloy compositions remained ductile and formable at temperatures as low as -58°F; whereas, two ODS molybdenum alloy compositions via Procedure B remained ductile at temperatures as low as -13°F.

ODS Alloy Key: (for tables and figures)

2 or 4 → volume percent oxide
C, Y, or L → oxide particle dispersant
C = CeO_2, Y = Y_2O_3, L = La_2O_3,
D or W → Powder Preparation Method
W = Procedure B, D = Procedure A
I → In-Process Anneal

References:

a. WADC Technical Report 54-398 dated January 1955, "Investigation of Molybdenum and Molybdenum-Base Alloys Made by Powder-Metallurgy Techniques"
b. AFML-TR-65-407 Part II dated November 1966, "Development of Dispersion Strengthened Tungsten-Base Alloys"
c. PB-151-099 dated November 1960, "Physical and Mechanical Properties of Commercial Molybdenum-Base Alloys"
d. U. S. Patent Number 4,950,327, dated August 21, 1990.
e. Report Number P-1085-023, Contract: DE-AC03-92SF19441, Monthly Report for 2/1/94 and 3/1/94, Space Power, Inc.
f. G. M. Ault and H. M. Burte, in Oxide Dispersion Strengthening, (G. S. Ansell, T. D. Cooper, and F. V. Lenel, eds.) Gordon and Breech Science Publishers, Inc., New York (1968) pp. 3-57.
g. T. B. Massalski, Binary Alloy Phase Diagrams: Volume 2, Second Edition, ASM International, Materials Park, OH (1990) pp. 1089-1091.
h. Y. C. Zhou and M. N. Rahaman, J. Mater. Res., **8** No. 7 (1993) 1680.
i. K. Hara, Nippon Tungsten Rev., **18** (1985) 26.
j. T. S. Chou and H. K. D. H. Bhadeshia, Mater. Sci. Techn., **9** (1993) 890.

Table 1. ODS Molybdenum Alloy Test Matrix

Dispersant	Volume Percent		Powder Preparation Method	
	2	4	Procedure A	Procedure B
Ceria	x	x	x	x
Yttria	x	x	x	x
Lanthana	x	x	x	x

Table 2. ODS Molybdenum Alloys Processing Schedule

Step	Process Step	Diameter (inch)	Reduction in Area (%)	Preheat Temperature (°C)
1	Cold Isostatic Press	1.500	-	-
2	Hydrogen Sinter	1.180	38	3400-3550
3	Hand Swage	1.180 1.080 1.000 0.920 0.847 0.780	- 16 14 15 15 15	2415-2505
4	Machine Swage	0.735 0.680 0.580 0.485	11 14 27 30	2280-2460
		0.410 0.345	29 29	2235-2325
		0.285 0.235	32 32	2190-2280
5	Draw	0.195 0.156-0.163	31 31	885-930

Table 3. Chemical Analysis Results of As-Swaged, ODS Molybdenum Alloys

Alloy ID	Oxide Volume Percent	Nominal Composition (wt.%)				Calculated Oxide Volume Percent		Major Impurities (ppmw)				
		Y	Ce	La	O			Fe	Ni	Cr	Cu	K
2CD	2	-	1.14	-	0.21	(Ce_2O_3) 1.97	(CeO_2) 1.99	25	26	<20	<10	<10
2CW	2	-	1.17	-	0.22	2.02	2.04	23	24	"	"	"
4CD	4	-	2.40	-	0.46	4.12	4.17	26	26	"	"	"
4CW	4	-	2.24	-	0.43	3.85	3.89	31	35	"	"	"
2LD	2	-	-	1.06	0.18	1.93		31	28	"	"	"
2LW	2	-	-	1.07	0.20	1.95		29	30	"	"	"
4LD	4	-	-	1.94	0.41	3.52		36	33	"	"	"
4LW	4	-	-	1.72	0.32	3.13		34	36	"	"	"
2YD	2	0.77	-	-	-	1.97		56	27	"	"	"
2YW	2	0.72	-	-	0.22	1.84		28	38	"	"	15
4YD	4	1.57	-	-	-	3.97		43	26	"	"	<10
4YW	4	1.47	-	-	0.43	3.73		35	41	"	"	"

*Chemical analysis performed at Teledyne Wah Chang Albany, Oregon.

Table 4. Oxide Particle and Primary Grain Size of As-Sintered and As-Swaged ODS Molybdenum Alloy Billets

Alloy Composition	As-Sintered Alloys		As-Swaged Alloys			
	Average Grain Dia., μm	Oxide Particle Size, μm	Average Grain width, μm	Oxide Particle Size, μm	Oxide Location (IG or TG)	Average Particle Density (particles/cm^3)
2CD	28	2.82±1.37	14.11±2.20	4.29±2.01$	IG	4.84
4CD	25	3.47±2.68	15.49±1.42	3.88± 1.57$	"	13.1
2CW	96	1.13±0.56	0.75±0.18#	0.15±0.10$#	"	$1.13x10^5$
4CW	10	1.98±0.63	0.60±0.29#	0.23±0.15$#	"	$6.28x10^4$
2LD	24	2.76±1.44	11.29±1.48	0.80±0.91$	"	746
4LD	14	4.86±3.75	13.11±1.46	1.46±0.65$	"	245
2LW	49	1.73±0.65	0.50±0.30#	0.23±0.11$#	IG, TG	$3.14x10^4$
4LW	11.6	2.29±0.89	0.80±0.14#	0.45±0.28$#	", "	$8.38x10^3$
2YD	20	2.47±0.79	31.75±5.11	1.63±0.57	", "	88.2
4YD	22	2.69±1.36	30.24±5.39	1.32±0.88	", "	332
2YW	9.4	2.64±1.29	0.51±0.13#	0.16±0.08#	", "	$9.32x10^4$
4YW	8.5	2.91±1.76	0.65±0.27#	0.41±0.18#	", "	$1.11x10^4$
2YDI*	-	-	23.09±5.35	2.30±1.11	", "	31.4
4YDI*	-	-	29.33±3.18	2.39±1.20	", "	55.9

*In-process anneal at 3272°F (1800°C) for 1 min.
#Analytical/transmission electron microscopy results.
$Average width of plastically deformed oxide stringers.
IG=Intergranular and **TG**=Transgranular; **AE**=As-Extruded.

Table 5. Oxide Particle and Primary Grain Size of Intermediate Swaged ODS Molybdenum Alloy Rods and Comparison of Microhardness with Fully Swaged Alloys

Alloy Composition	Intermediate Swaged Alloy Rods				Fully Swaged	
	Sample Diameter, inches	Average Grain Diameter, μm	Oxide Particle Size, μm	Microhardness (VHN, 5 kg load)	Microhardness	
					VHN (5 kg)	KHN (500 gm)
2CD	0.580	11.07±3.87	11.59±3.77	199±6	-	250±10
4CD	0.580	15.63±4.17#	20.14±9.36	199±5	-	262±4
2CW	0.580	2.16±1.01#	1.69±0.59	208±5	254±5	270±7
4CW	0.580	5.01±0.82	2.24±0.51	224±2	292±5	303±7
2LD	0.485	16.74±3.95#	4.63±2.89	202±7	-	265±6
4LD	0.780	7.39±2.35	7.67±1.69	214±7	262±6	273±8
2LW	0.485	2.61±0.86	1.14±0.26	224±2	262±2	272±9
4LW	0.485	5.67±1.25	2.12±0.78	208±6	289±5	285±4
2YD	-	-	-	-	-	265±7
4YD	-	-	-	-	-	272±10
2YW	-	-	-	-	261±2	297±3
4YW	-	-	-	-	297±6	312±3
2YDI*	-	-	-	-	-	287±8
4YDI*	-	-	-	-	-	272±7

*In-process anneal at 3270°F (1800°C) for 1 minute.
#Subgrains observed in optical photomicrograph.

Table 6. Recrystallization Temperature of As-Swaged, ODS Molybdenum Alloys, Commercial Molybdenum Alloys, and Other ODS Systems, References (c) and (f).

Alloy ID	Alloy Composition	Recrystallization Temperature, °F	Normalized Temperature, RXT/T_m
2CD	2 vol.% Ceria, D	2012	0.43
4CD	4 vol.% " , "	2192	0.46
2CW	2 vol.% " , W	3092	0.65
4CW	4 vol.% " , "	3992	0.84
2LD	2 vol.% Lanthana, D	2012	0.43
4LD	4 vol.% " , "	3452	0.73
2LW	2 vol.% " , W	3092	0.65
4LW	4 vol.% " , "	3992	0.84
2YD	2 vol.% Yttria, D	1832	0.38
4YD	4 vol.% " , "	"	"
2YDI	2 vol.% " , D-In Proc.	"	"
4YDI	4 vol.% " , " "	"	"
2YW	2 vol.% " , W	2732	0.58
4YW	4 vol.% " , "	2552	0.53
Unalloyed Mo	Mo-0.01C w/o	2150	0.45
Mo TZC	Mo-1.25Ti-0.15Zr-0.15C w/o	2800	0.59
MoReHfC	Mo-2.0Re-0.5HfC w/o	3050	0.67
ThDW	W-3.8 vol.% ThO_2	5252	0.86
TDNi	Ni-2.0 vol.% ThO_2	2462	0.94

Note: Recrystallization temperature determined from both micro-hardness drop and post-anneal metallography.

Figure 7. Room Temperature (78°F) Tensile Data of As-Swaged, ODS Molybdenum Alloy Rods Loaded to Failure at a Strain Rate of 0.05 min^{-1} or $8.33x10^{-4}$ sec^{-1}

No.	Sample Composition	Surface Treatment	0.2 % Yield Stress (psi)	Ultimate Tensile Strength (psi)	Elongation to Failure (%)	Reduction in Area (%)
Control	Unalloyed Molybdenum, 5/8" bar	As-Machined	78,800	102,000	40	61.1
1	2 vol.% Ceria, W	"	107,031	118,750	13.1	57.8
2	" " ", D	"	100,000	111,719	13.1	62.5
3	" " ", "	Electropolished	98,825	109,206	12.6	60.3
4	4 vol.% Ceria, W	As-Machined	140,476	159,206	7.1	54.0
5	" " ", D	"	108,125	119,063	10.1	46.9
6	2 vol.% Lanthana, W	"	107,936	119,841	13.0	58.7
7	" " ", D	"	107,936	122,540	15.0	61.9
8	" " ", "	Electropolished	106,031	119,841	12.9	63.5
9	4 vol.% Lanthana, W	As-Machined	132,031	148,438	7.6	29.7
10	" " ", D	"	110,317	126,984	9.7	47.6
11	2 vol.% Yttria, W	"	128,571	138,889	13.6	49.2
12	" " ", D	"	109,375	115,625	11.2	48.4
13	" " ", "	Electropolished	98,412	111,111	11.9	49.2
14	4 vol.% Yttria, W	As-Machined	128,095	142,857	5.9	41.3
15	" " ", D	"	103,492	117,460	10.4	49.2
16	2 vol.% Yttria, D-In	"	101,612	109,677	11.1	43.5
17	" " ", " "	Electropolished	94,032	106,452	10.3	48.4
18	4 vol.% Yttria, " "	As-Machined	98,888	109,524	6.7	34.9

Table 8. Room Temperature Tensile Data of ODS Molybdenum Alloy Rods Vacuum Annealed at 3630°F for One Hour Loaded to Failure at a Strain Rate of 0.05 min^{-1} or $8.33x10^{-4}$ sec^{-1}.

No.	Sample Composition	0.2% Yield Stress (psi)	Ultimate Tensile Stress (psi)	Uniform Elongation (%)	Elongation to Failure (%)	Reduction in Area (%)
1	2 vol.% Ceria, W	56,463	76,852	9.25	25.41 (A)	59.84
2	4 ", ", "	73,559	105,554	18.89	38.97 (A)	56.39
3	2 vol.% Lanthana, W	52,816	76,552	10.17	28.92	65.19
4	4 ", ", "	72,770	100,938	16.29	33.61	56.49
5	2 vol.% Yttria, W	61,461	89,913	8.36	8.36	9.54
6	4 ", ", "	70,568	100,238	14.51	22.30 (A)	25.70

(A) Failed outside middle half of gauge length.

Table 9. Ductile-to-Brittle Transition Temperatures (DBTT) of ODS Molybdenum Alloy Rods Loaded to Failure at a Strain Rate of 0.05 min^{-1} or $8.33x10^{-4}$ sec^{-1}.

Sample Composition	Ductile-to-Brittle Transition Temperature, °F	
	As-Swaged	One Hour Vacuum Anneal at 3630°F
2 vol.% Ceria, W	-103	122
" " ", D	<-148	-
4 vol.% Ceria, W	-148	-58
" " ", D	"	-
2 vol.% Lanthana, W	-103	122
" " ", D	<-148	-
4 vol. Lanthana, W	"	-13
" " ", D	"	-
2 vol.% Yttria, W	"	212
" " ", D	-148	-
4 vol.% Yttria, W	"	212
" " ", D	"	-
2 " ", " (A)	-58	-
4 " ", " (A)	"	-

(A) In-process anneal at 3270°F for 1 minute.

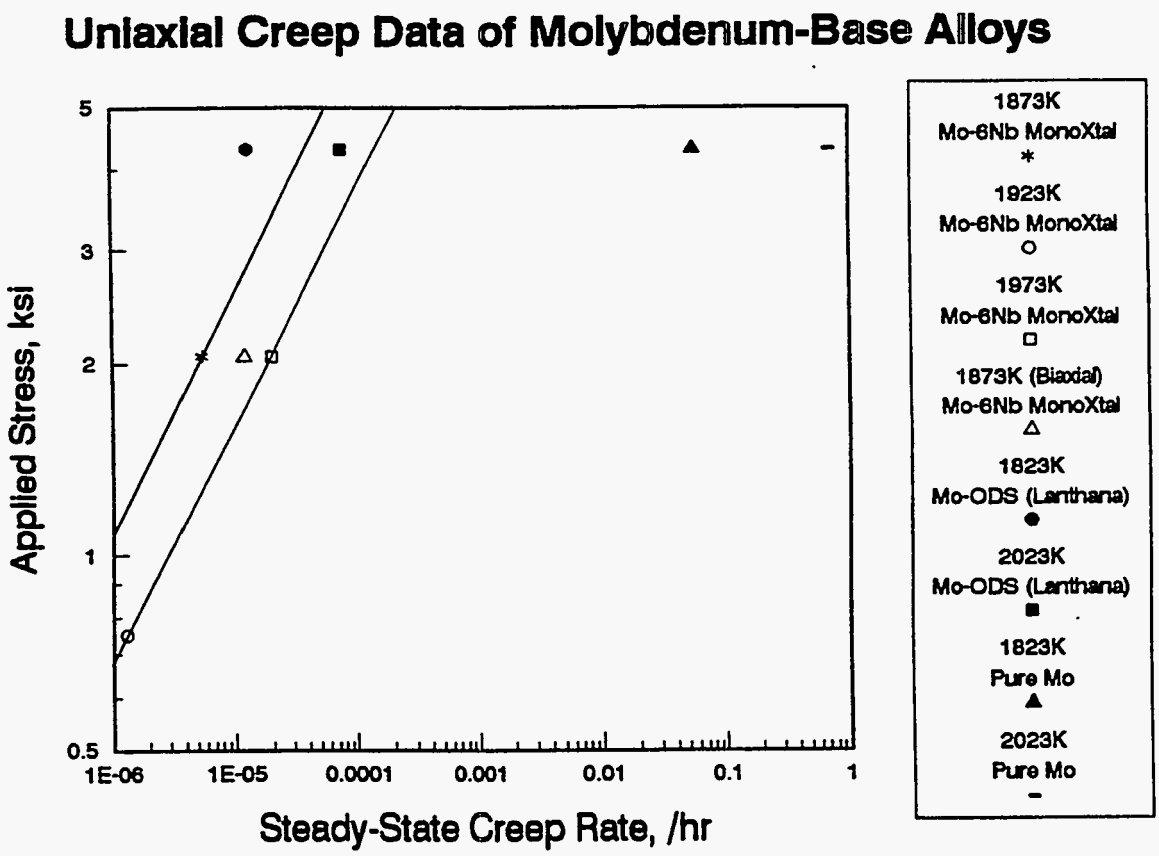

Figure 1. Graphic comparison of uniaxial steady-state creep rates of a commercial ODS molybdenum alloy, unalloyed molybdenum, and a monocrystalline molybdenum - 6 wt.% niobium alloy, Reference (e).

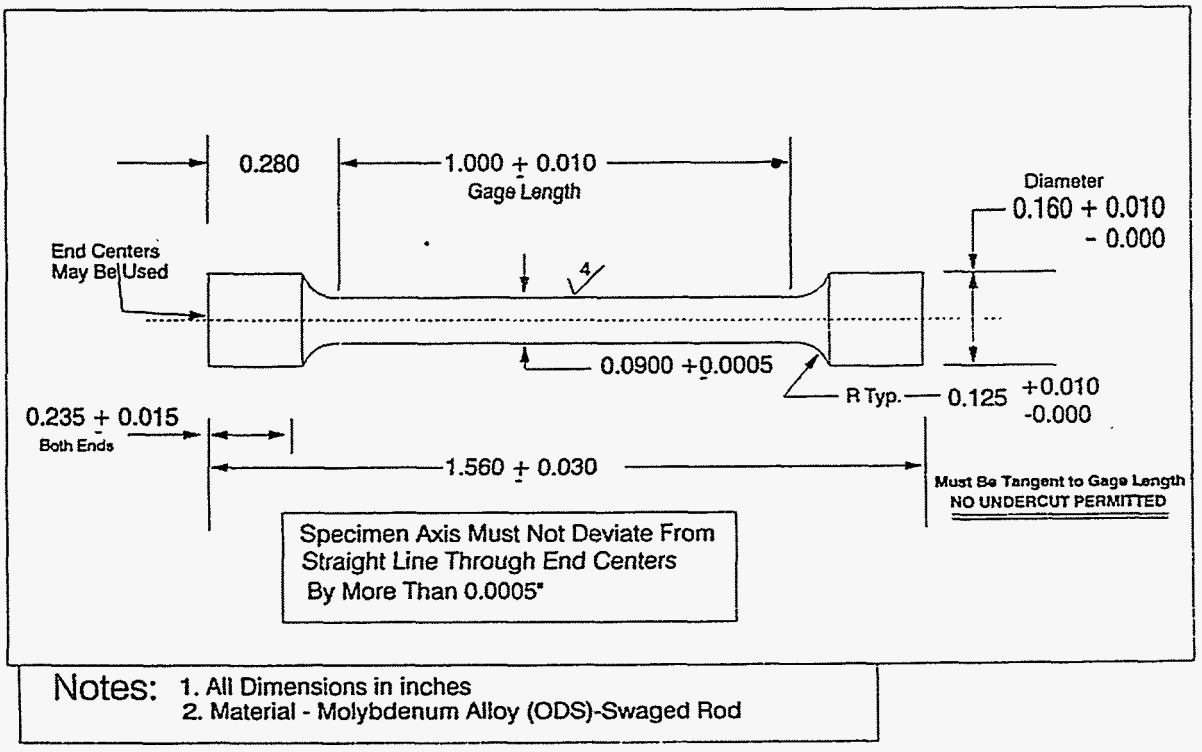

(a)

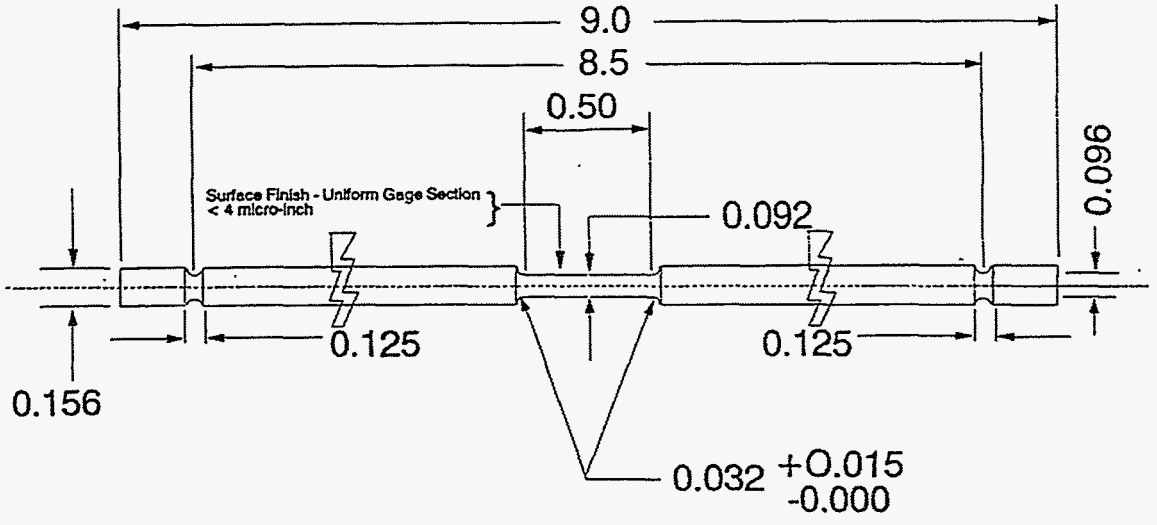

(b)

Figure 2. Industrial drawing of (a) room temperature (DBTT) and (b) elevated temperature tensile specimens.

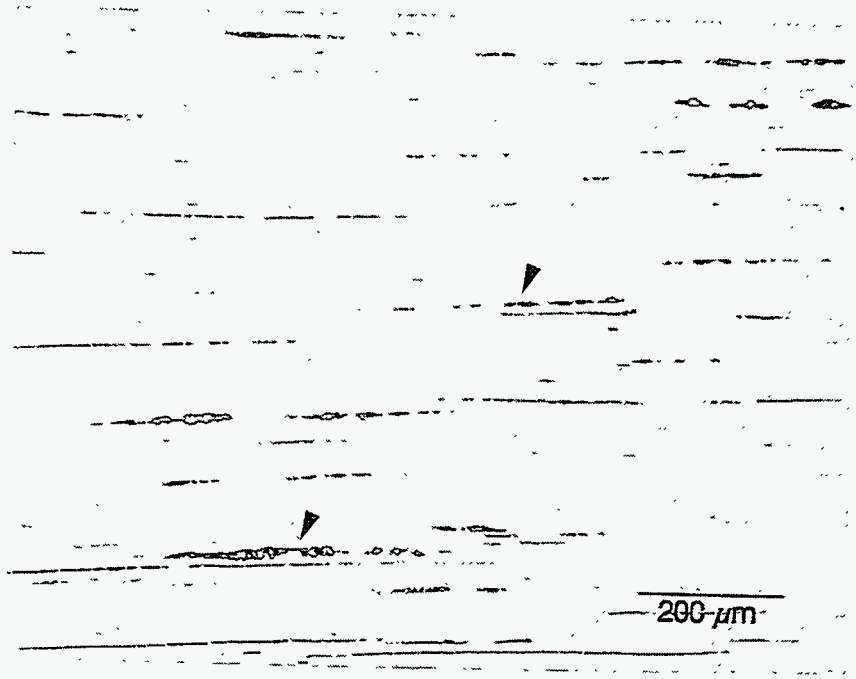

(a)

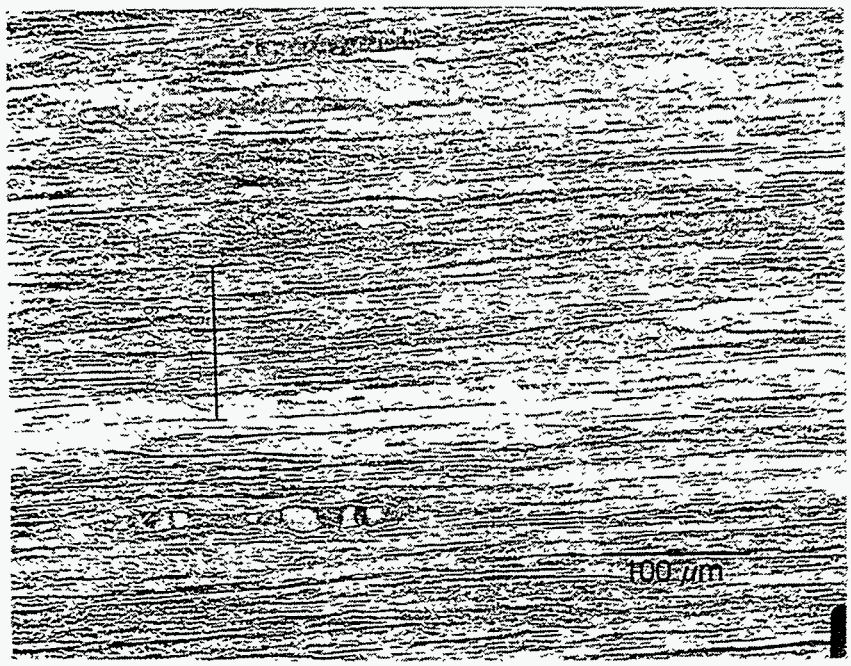

(b)

Figure 3. Optical photomicrograph of as-swaged ODS molybdenum alloy via Procedure A containing 2 volume percent of ceria: (a) unetched and (b) etched with Murakami's etchant.

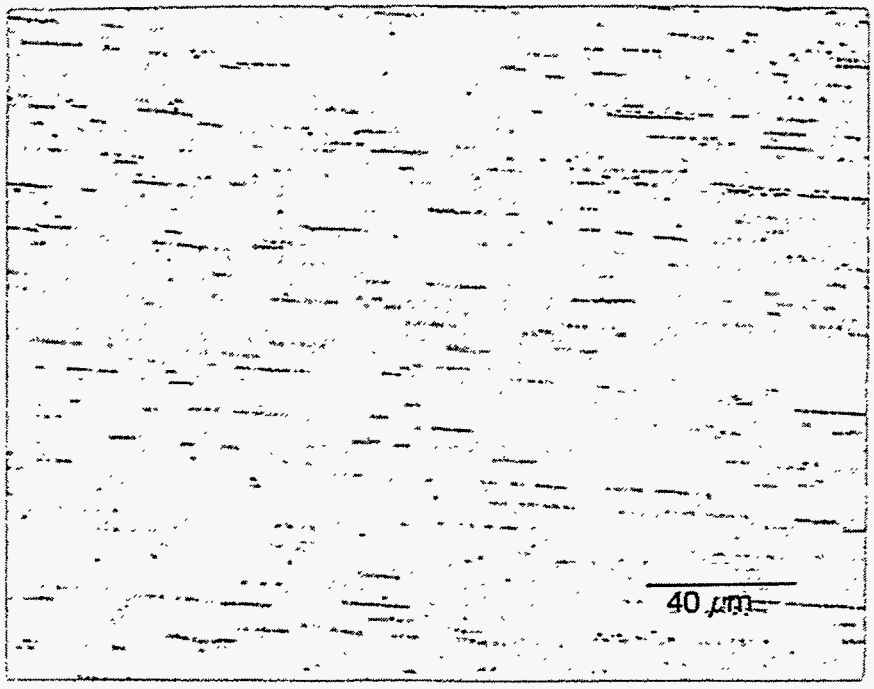

(a)

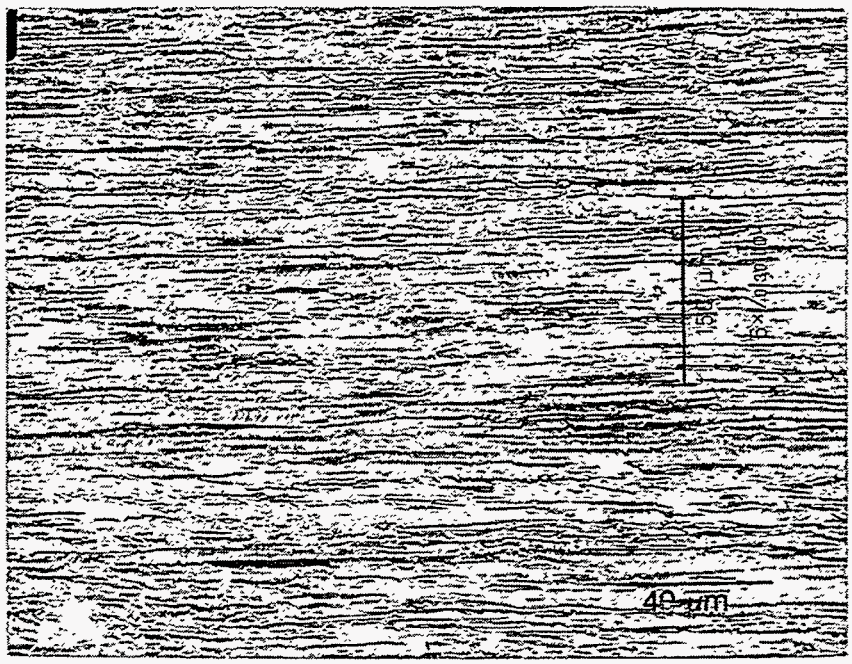

(b)

Figure 4. Optical photomicrograph of as-swaged ODS molybdenum alloy via Procedure B containing 2 volume percent of ceria: (a) unetched and (b) etched with Murakami's etchant.

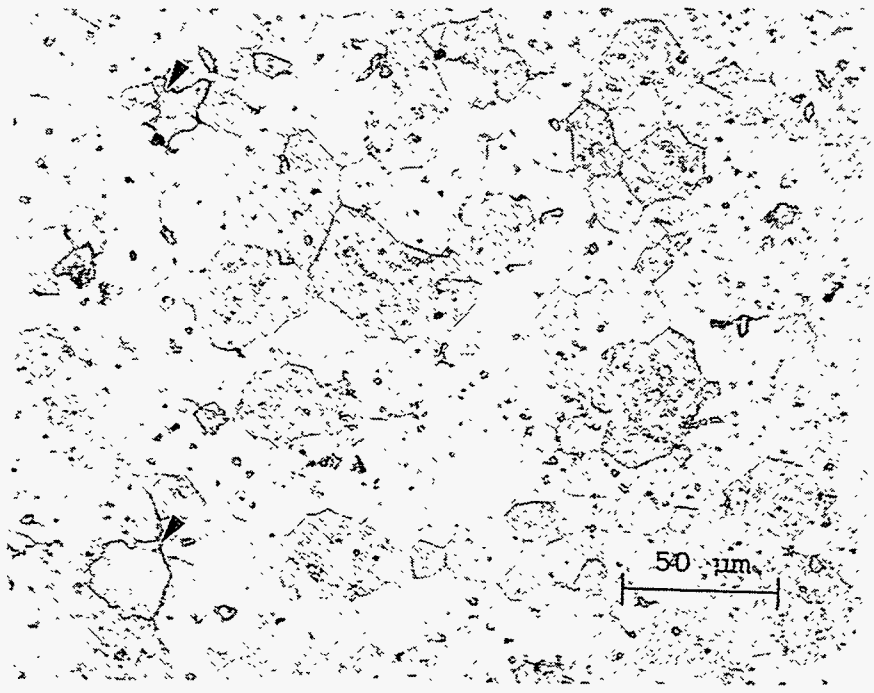

(a)

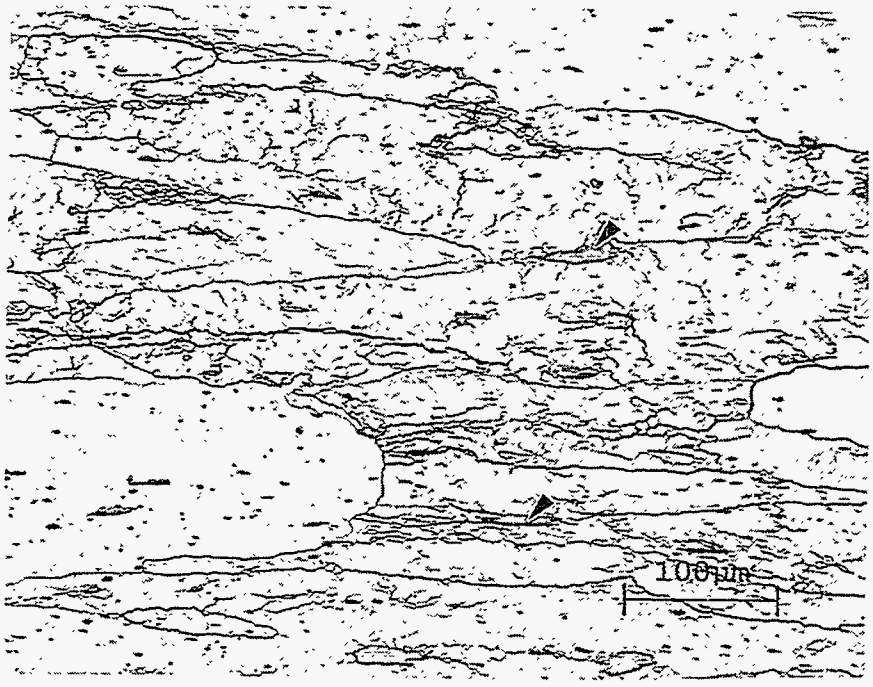

(b)

Figure 5. Optical photomicrograph of ODS molybdenum alloy via Procedure A containing 2 volume percent of ceria: (a) as-sintered and (b) intermediate swaged rod, 0.580 inch diameter.

Figure 6. Brightfield electron micrograph of ODS molybdenum alloy via Procedure B containing four volume percent ceria (transverse orientation).

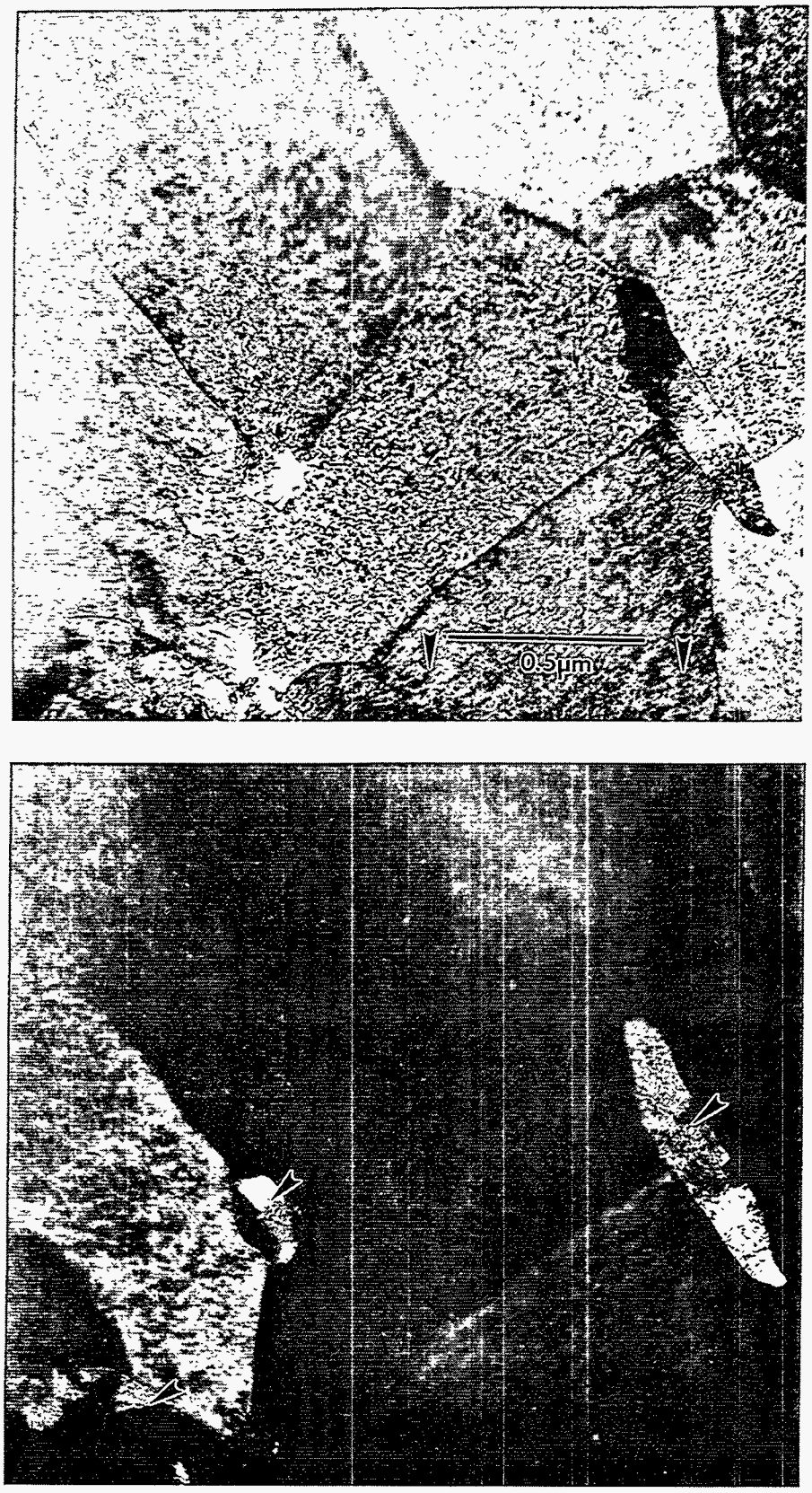

Figure 7. Brightfield and darkfield electron micrograph of ODS molybdenum alloy via Procedure B containing four volume percent ceria (transverse orientation).

Figure 8. Brightfield electron micrograph of ODS molybdenum alloy via Procedure B containing four volume percent yttria (longitudinal orientation). **Note:** Microvoids evident between the non-deformable yttria particle and the molybdenum grains.

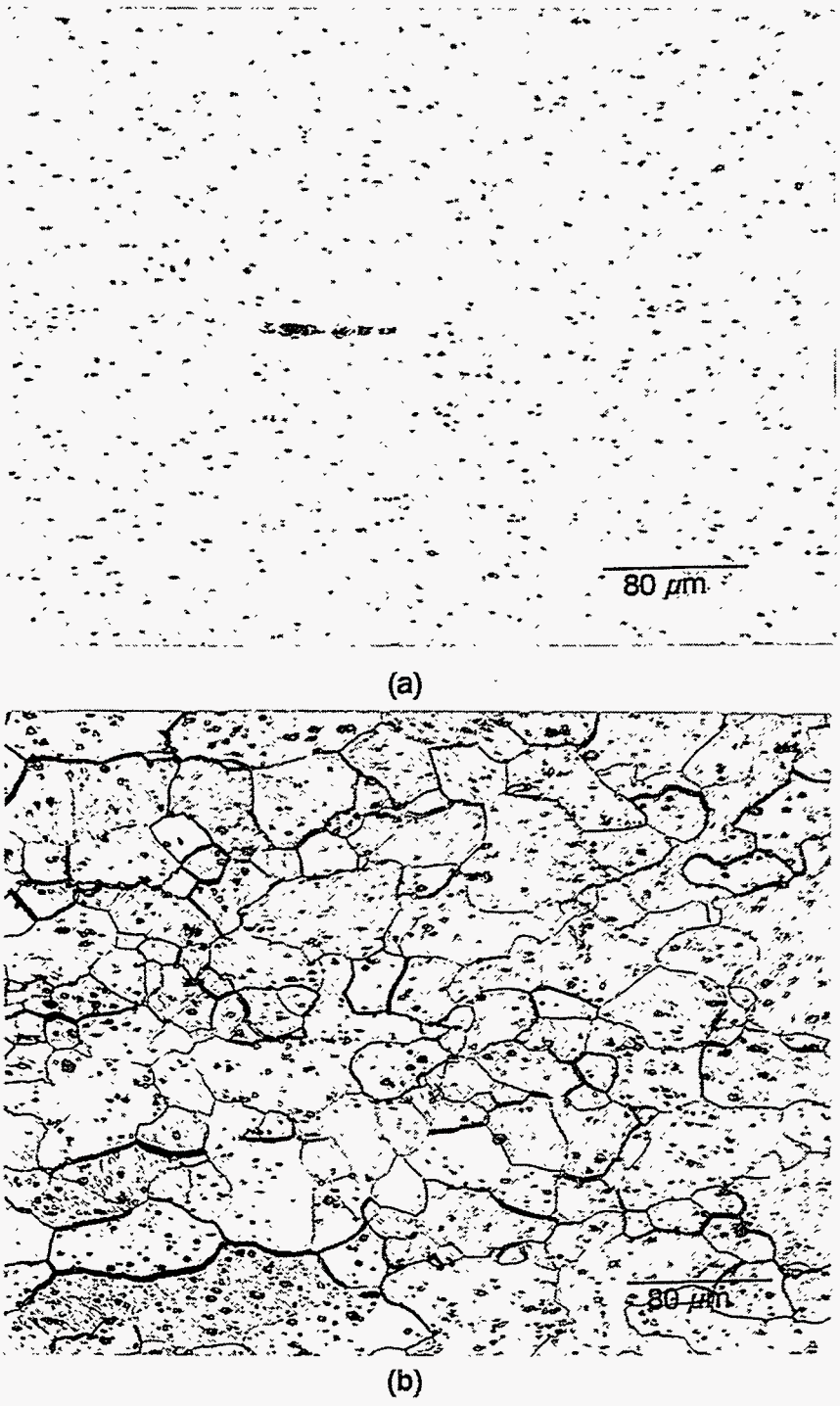

Figure 9. Optical photomicrograph of ODS molybdenum alloy via Procedure A containing 2 volume percent of yttria vacuum annealed at 3270°F for one hour: (a) unetched and etched with Murakami's etchant.

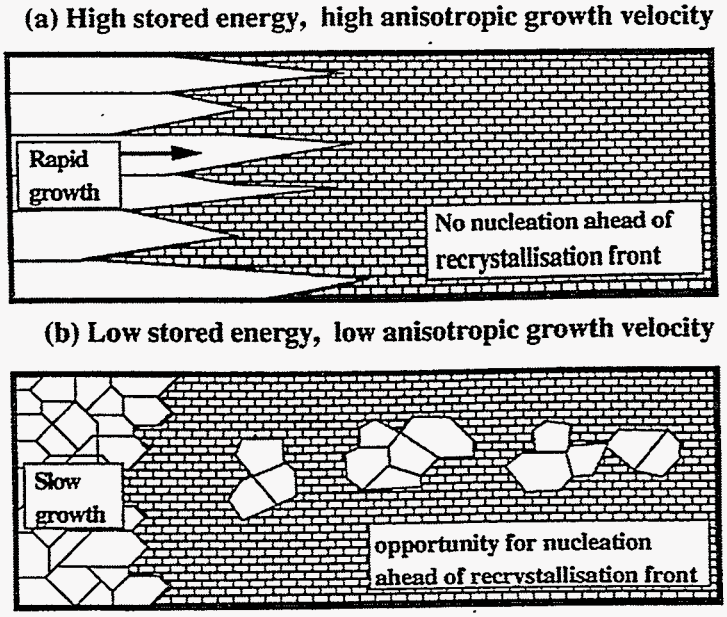

1 Schematic development of recrystallisation process for *a* high and *b* low stored energy

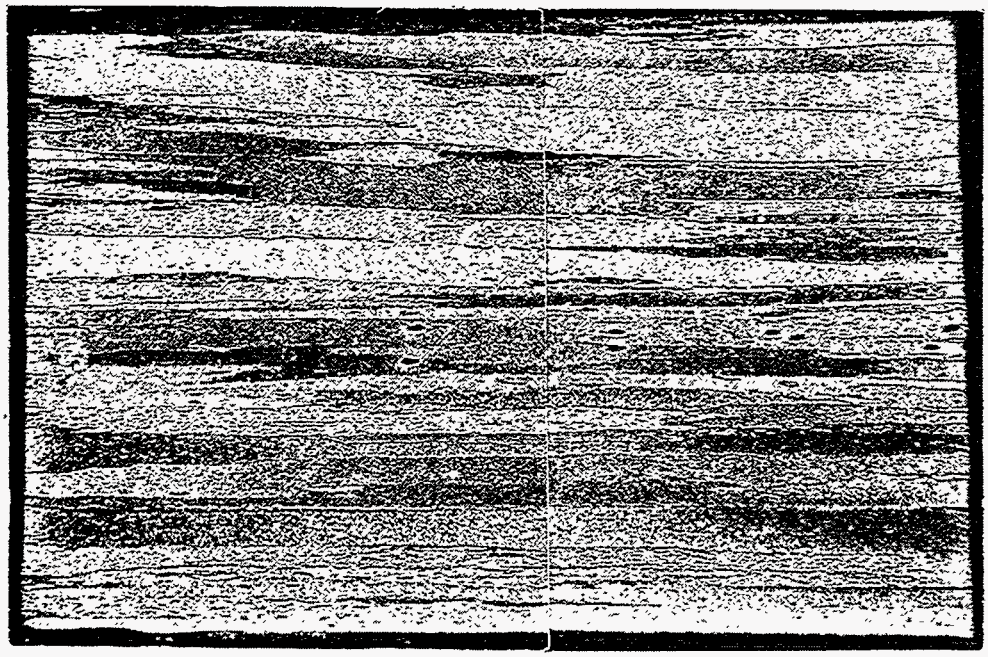

20x

Figure 10. Schematic illustration of recrystallization process for (a) high and (b) low stored energy, Reference (j), and an optical photomicrograph of ODS molybdenum alloy via Procedure B containing 2 volume percent of ceria vacuum annealed at 3270°F for one hour.

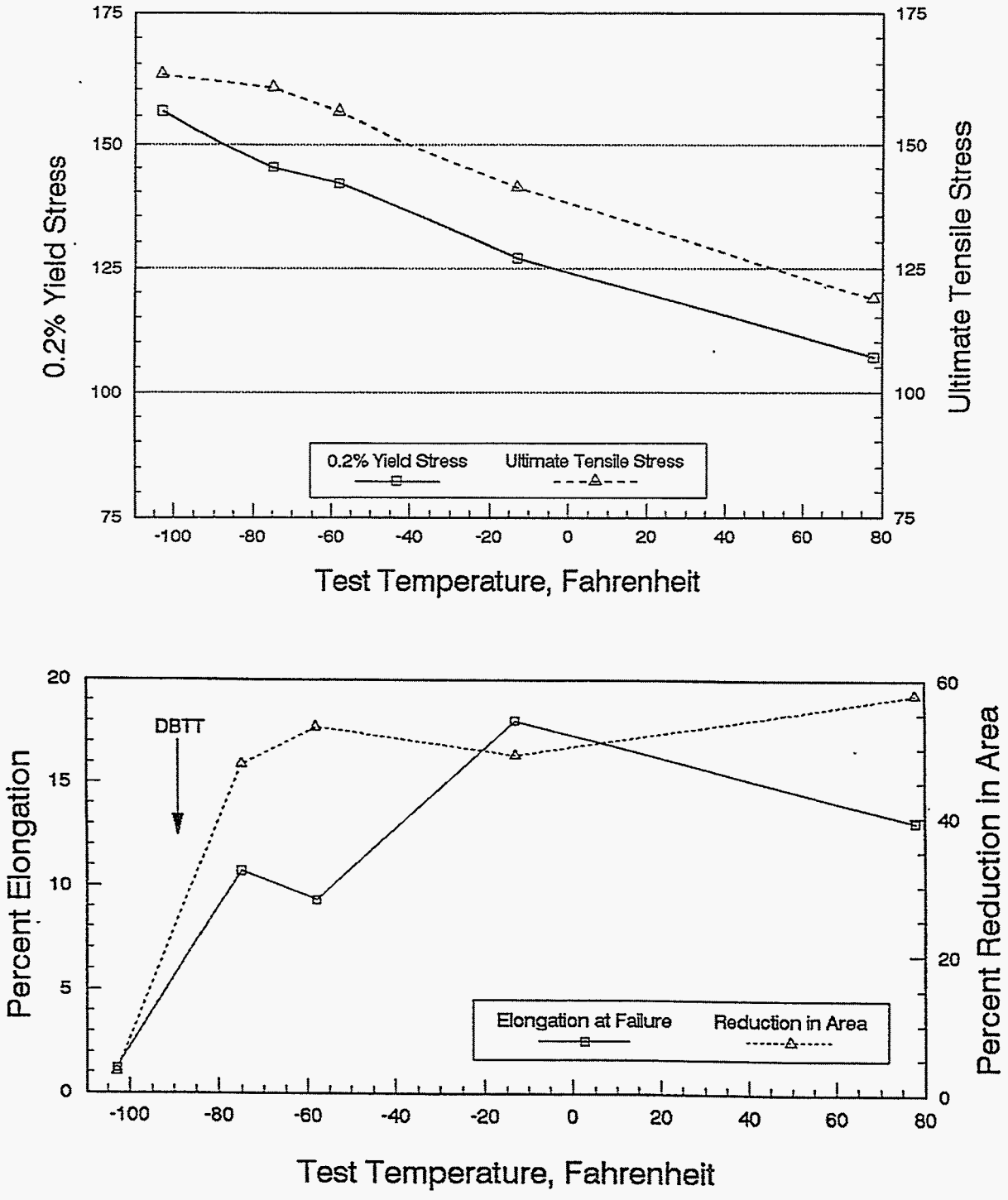

Figure 11. Uniaxial tensile results of ODS molybdenum alloy via Procedure B containing 2 volume percent ceria particles in the as-swaged condition: crosshead speed 0.05 in/min.

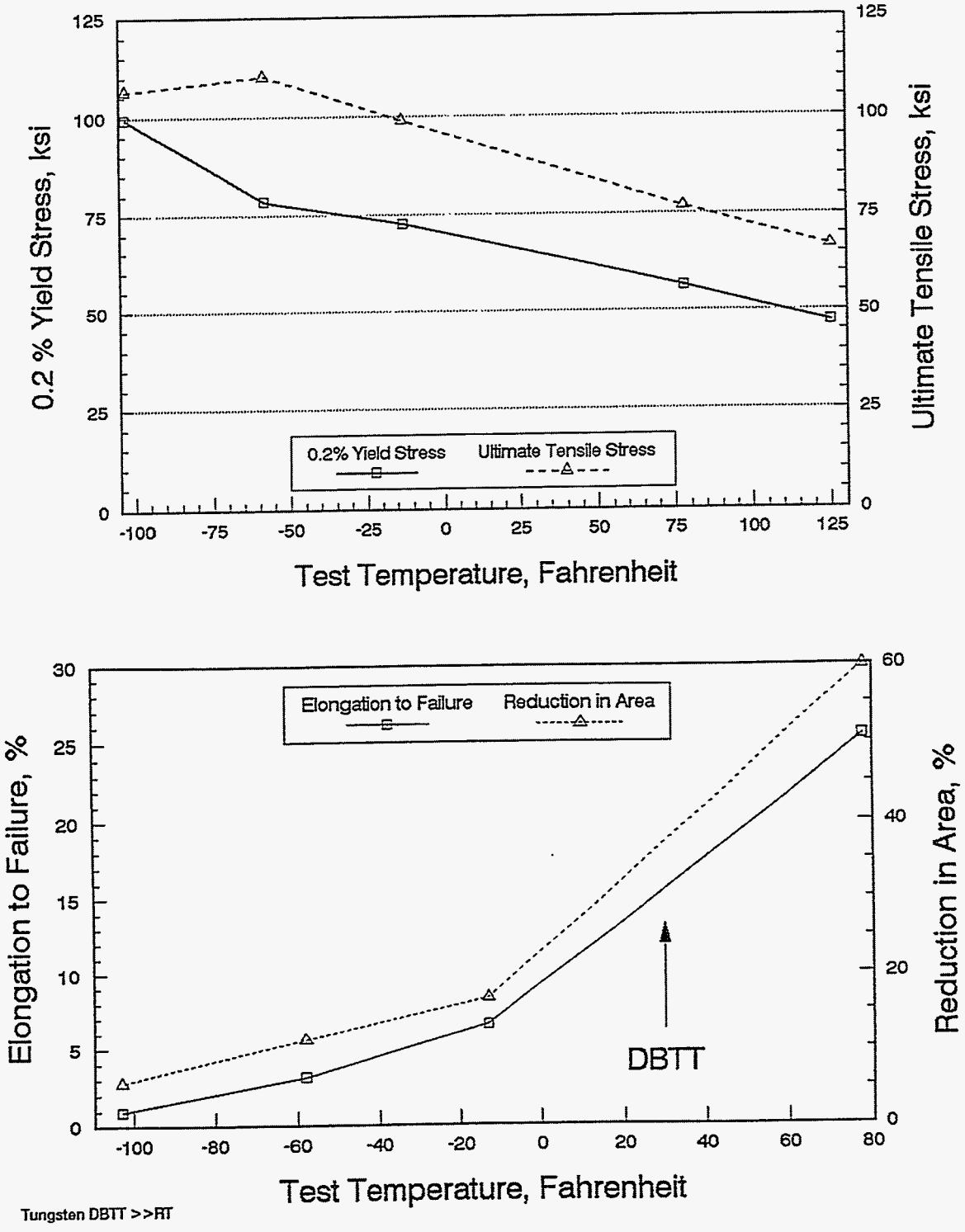

Figure 12. Uniaxial tensile results of ODS molybdenum alloy via Procedure B containing 2 volume percent ceria particles vacuum annealed at 3630°F for one hour: crosshead speed 0.05 in/min.

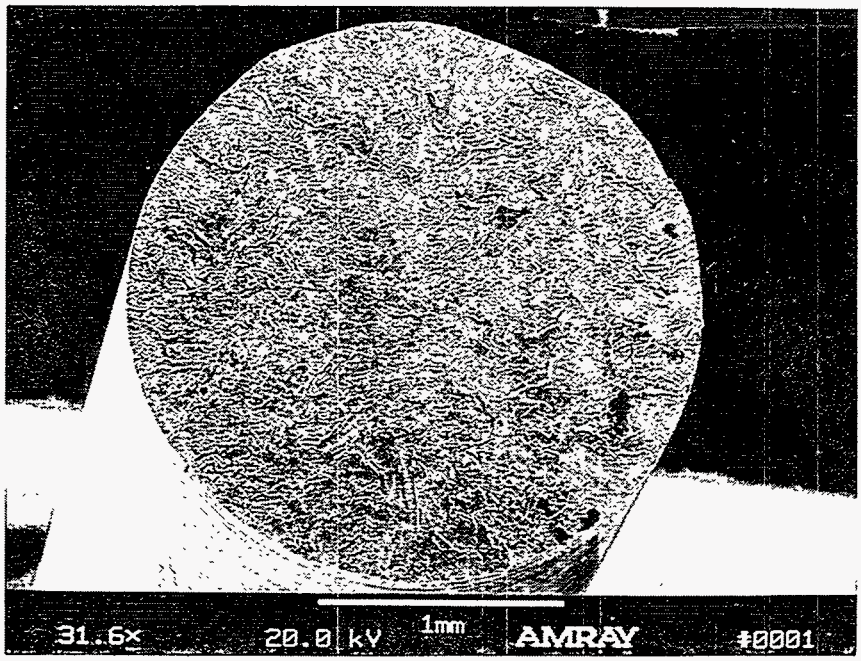

(a)

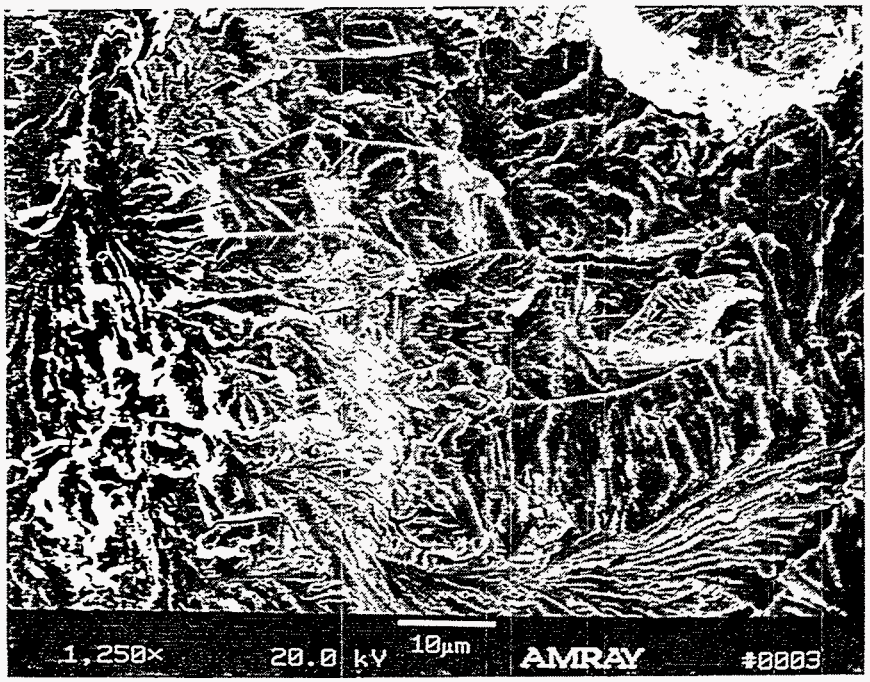

(b)

Figure 13. Secondary electron micrograph of a fracture surface from an as-swaged ODS molybdenum alloy containing 2 volume percent ceria via Procedure B uniaxially loaded to failure at -103°F: (a) low and (b) high magnification.

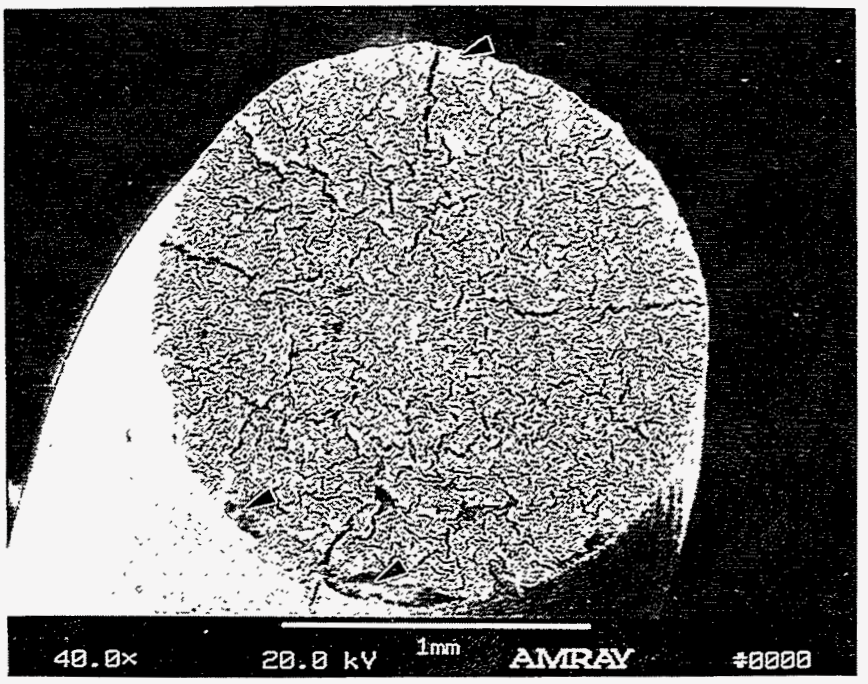

(a)

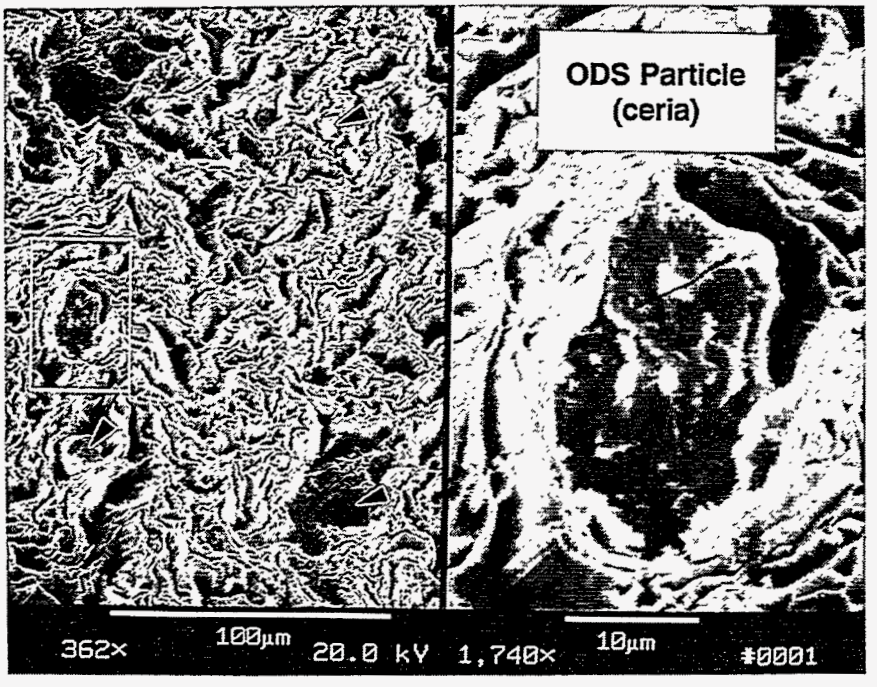

(b)

Figure 14. Secondary electron micrograph of a fracture surface from an as-swaged ODS molybdenum alloy containing 2 volume percent ceria via Procedure A uniaxially loaded to failure at -103°F: (a) low and (b) high magnification.

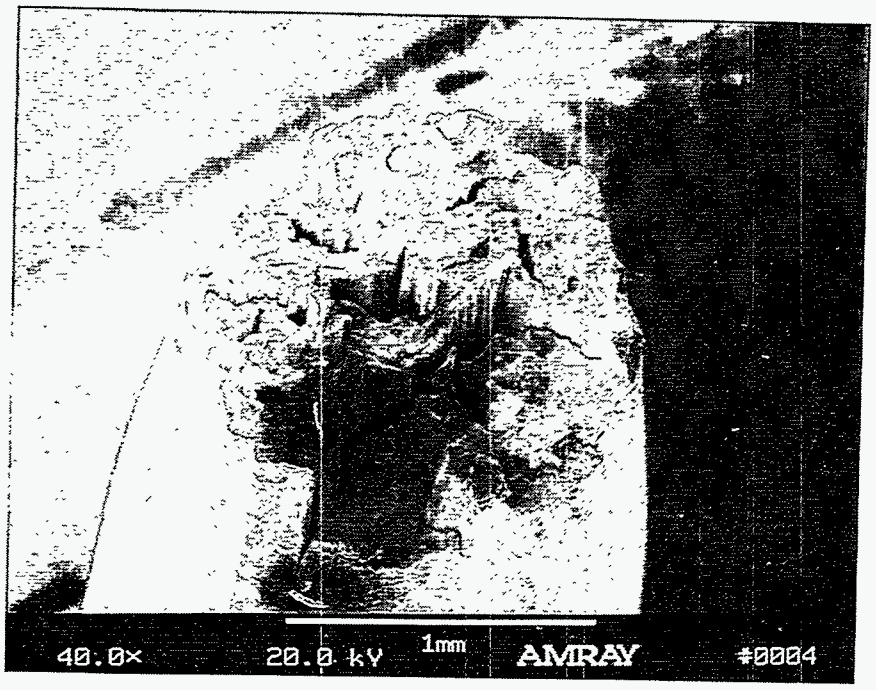

(a)

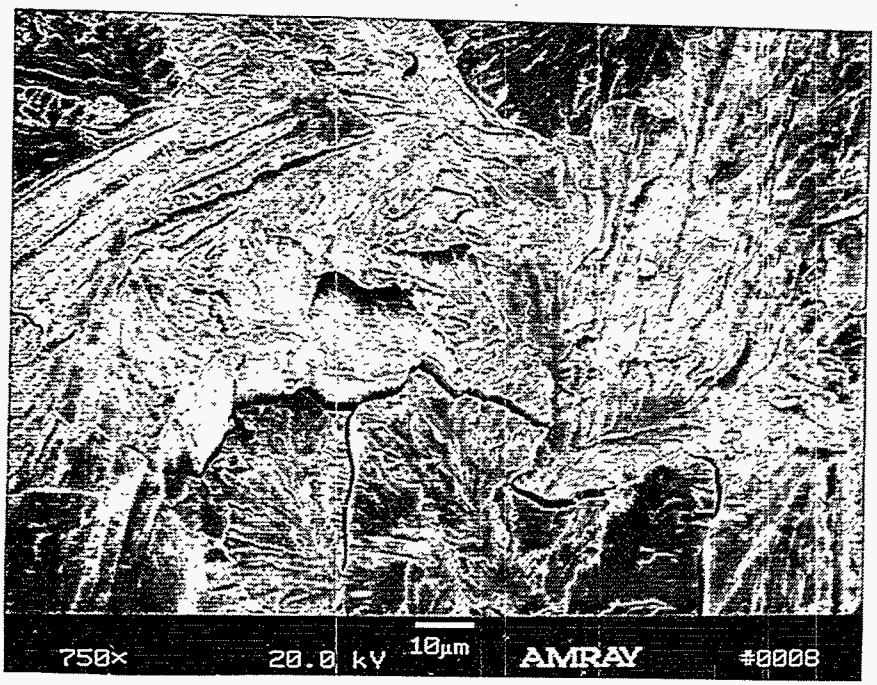

(b)

Figure 15. Secondary electron micrograph of a fracture surface from a vacuum annealed (3630°F for one hour), ODS molybdenum alloy containing 2 volume percent ceria via Procedure B uniaxially loaded to failure at room temperature (78°F): (a) low and (b) high magnification.

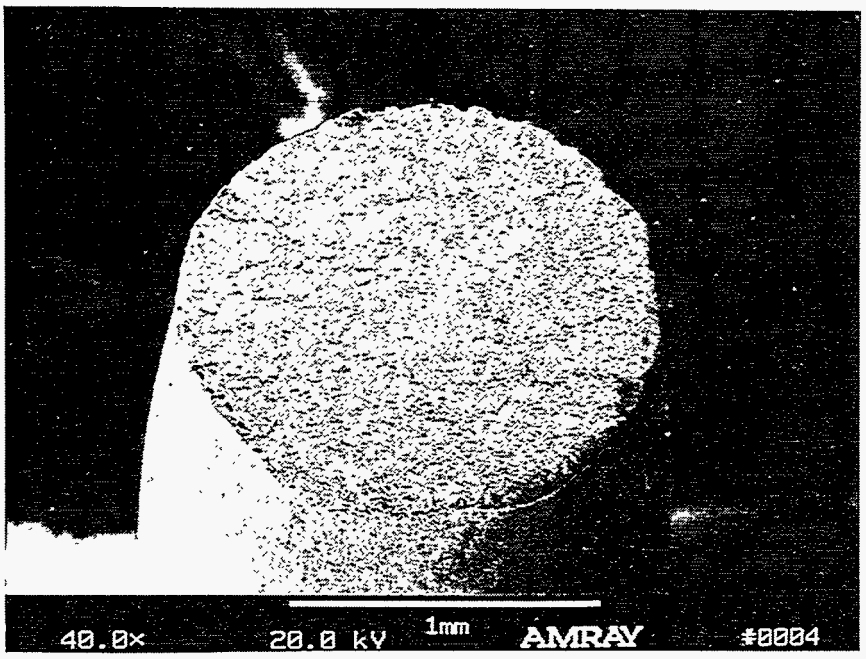

(a)

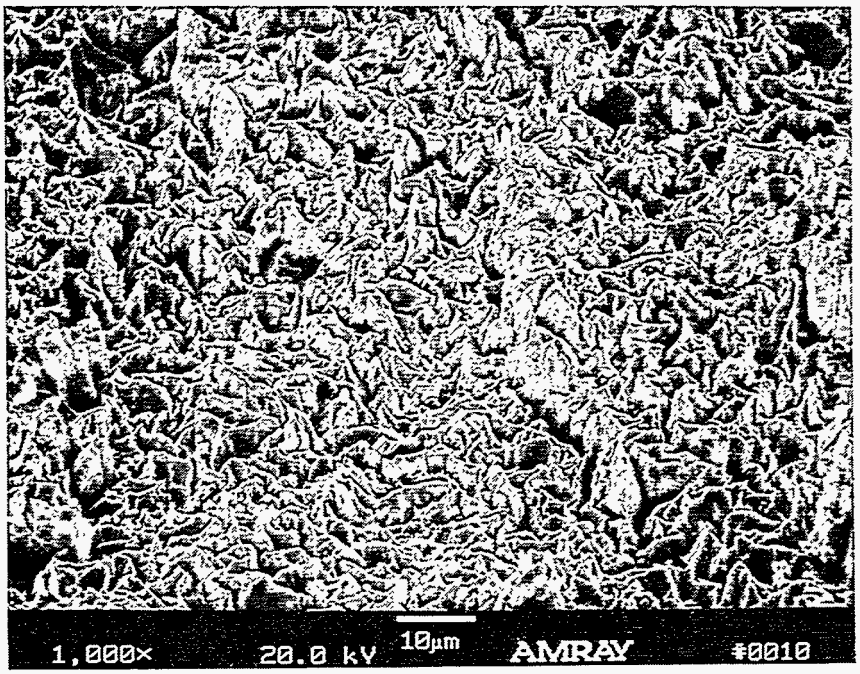

(b)

Figure 16. Secondary electron micrograph of a fracture surface from a vacuum annealed (3630°F for one hour), ODS molybdenum alloy containing 4 volume percent ceria via Procedure B uniaxially loaded to failure at room temperature (78°F): (a) low and (b) high magnification.

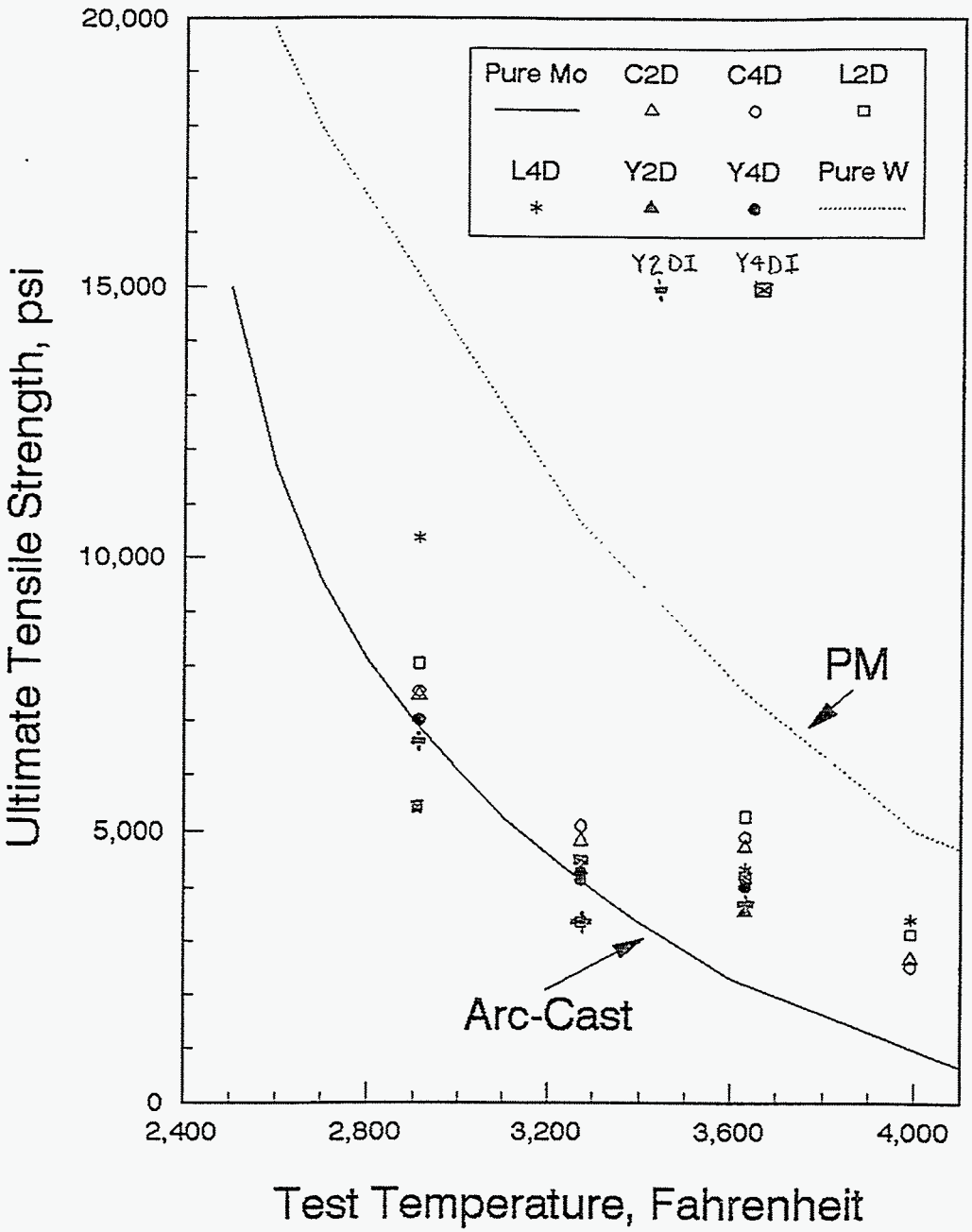

Figure 17. The effect of test temperature on the ultimate tensile stress of ODS molybdenum alloys via Procedure A and commercial unalloyed molybdenum and powder metallurgy tungsten rod, References (c) and (f).

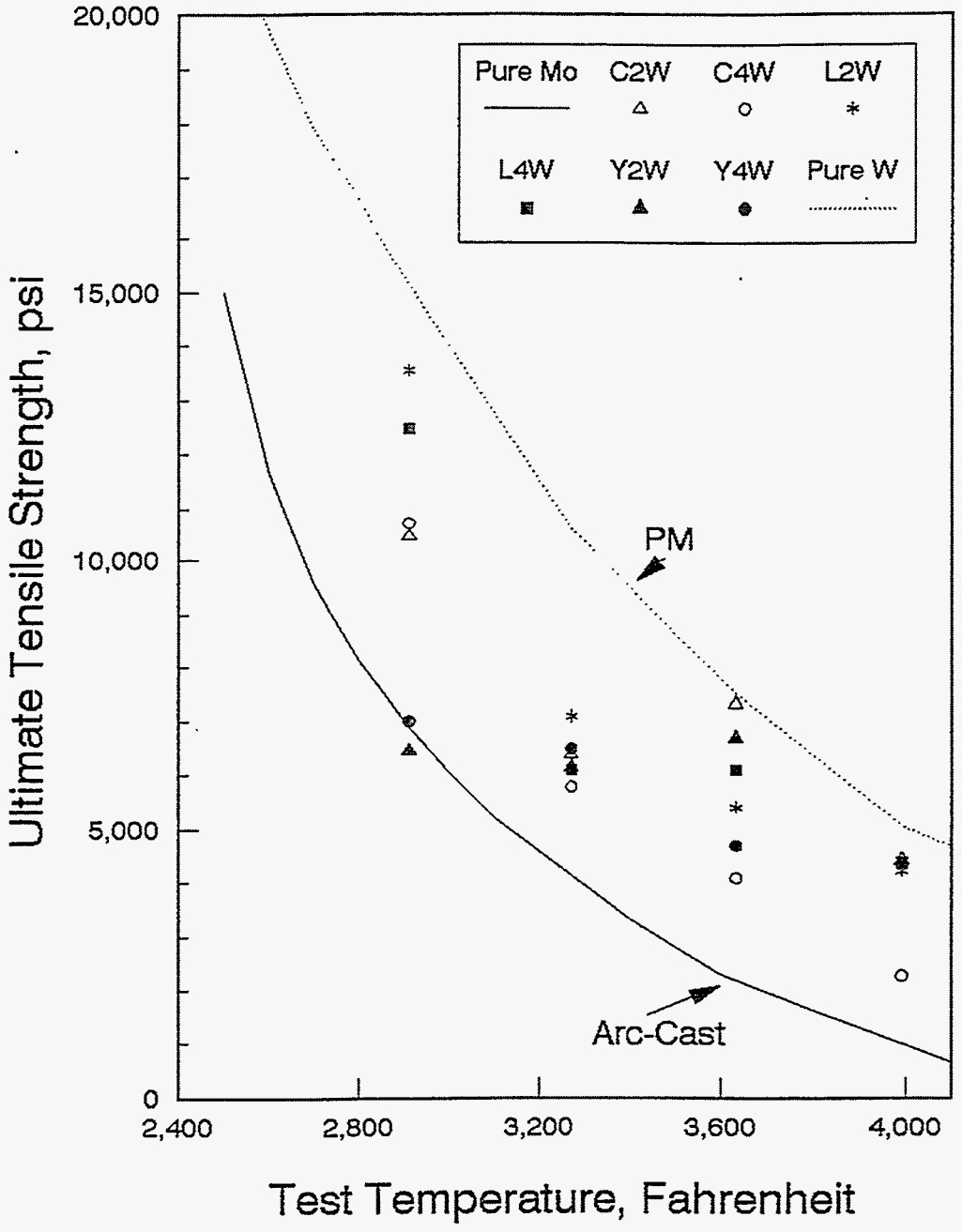

Figure 18. The effect of test temperature on the ultimate tensile stress of ODS molybdenum alloys via Procedure B and commercial unalloyed molybdenum and powder metallurgy tungsten rod, References (c) and (f).

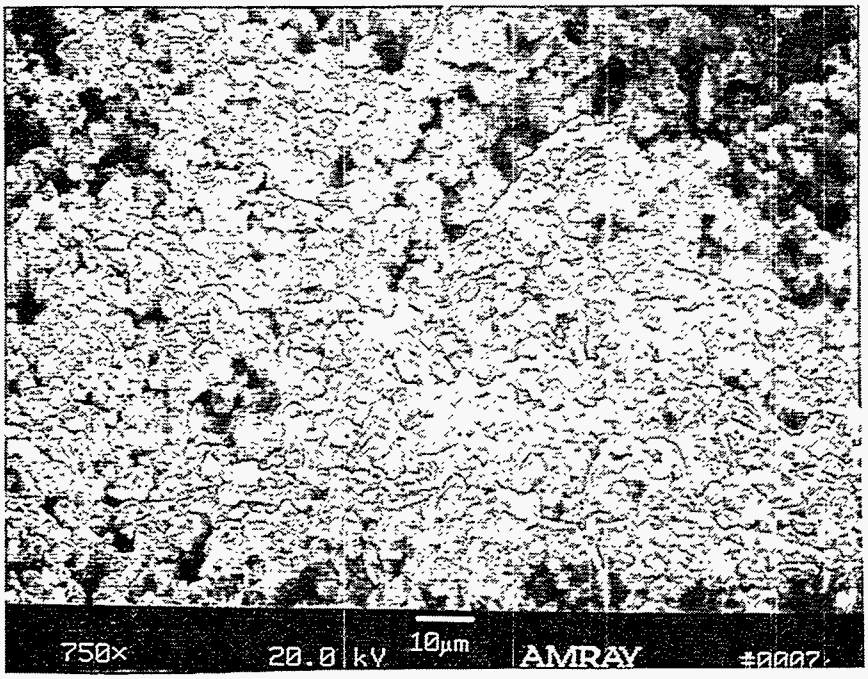

(a)

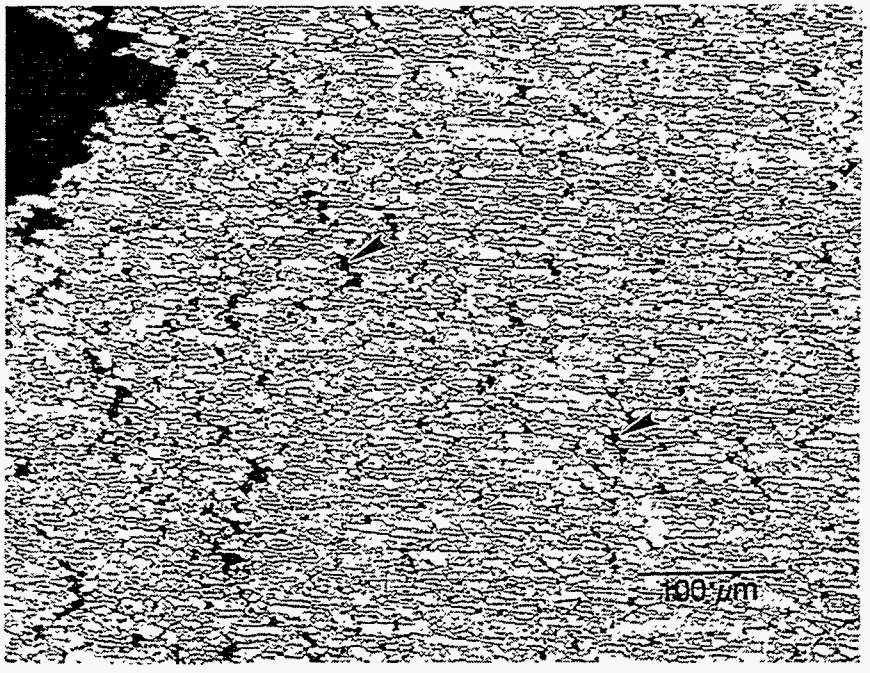

(b)

Figure 19. (a) Secondary electron and (b) optical micrographs of a fracture surface from ODS molybdenum alloy containing 4 volume percent ceria via Procedure B uniaxially loaded to failure at 2910°F in dynamic vacuum ($<10^{-5}$ torr).

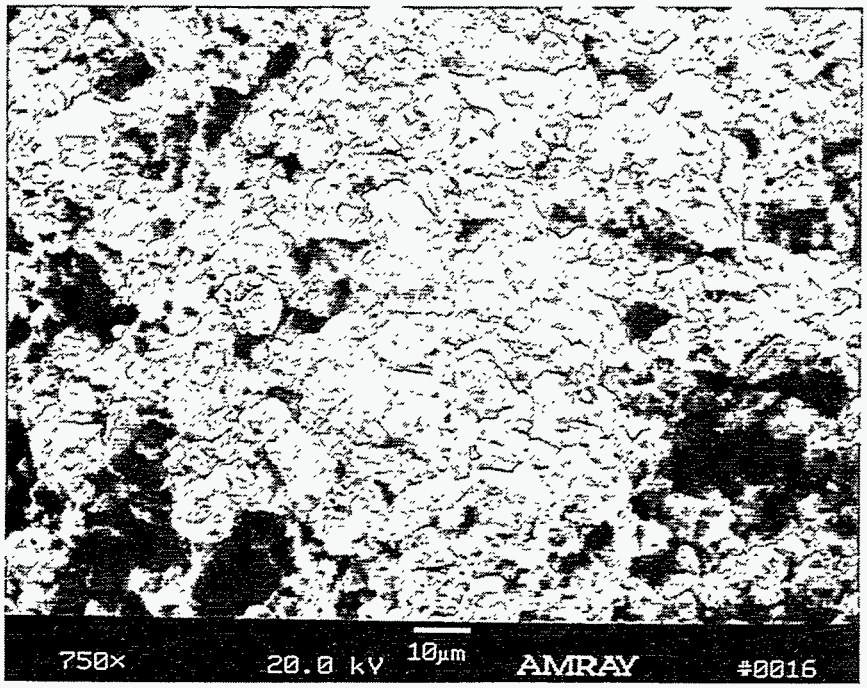

(a)

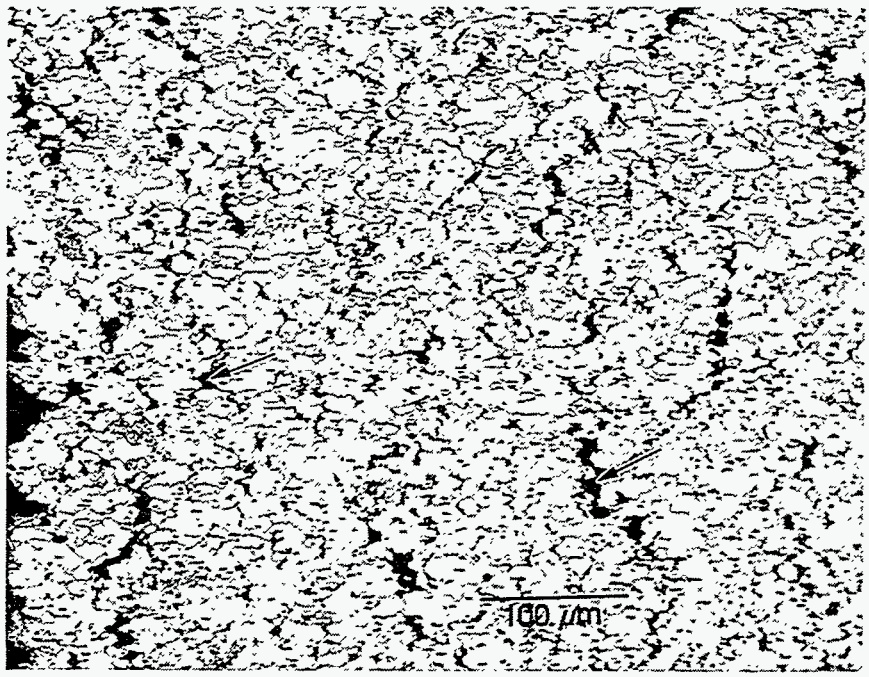

(b)

Figure 20. (a) Secondary electron and (b) optical micrographs of a fracture surface from ODS molybdenum alloy containing 4 volume percent yttria via Procedure B uniaxially loaded to failure at 2910°F in dynamic vacuum ($<10^{-5}$ torr).